Functional assessment of the "two-hit" model for neurodevelopmental defects in *Drosophila* and *X. laevis*

Short title: Assessment of "two-hit" model for developmental defects

Lucilla Pizzo[1]*, Micaela Lasser[2]*, Tanzeen Yusuff[1], Matthew Jensen[1], Phoebe Ingraham[1], Emily Huber[1], Mayanglambam Dhruba Singh[1], Connor Monahan[2], Janani Iyer[1], Inshya Desai[1], Siddharth Karthikeyan[1], Dagny J. Gould[1], Sneha Yennawar[1], Alexis T Weiner[1], Arjun Krishnan[4,5], Melissa Rolls[1], Laura Anne Lowery[6] and Santhosh Girirajan[1,3#]

1. Department of Biochemistry and Molecular Biology, The Pennsylvania State University, University Park, PA USA
2. Department of Biology, Boston College, Chestnut Hill, MA USA
3. Department of Anthropology, The Pennsylvania State University, University Park, PA USA
4. Department of Computational Mathematics, Science and Engineering, Michigan State, University, East Lansing, MI, USA
5. Department of Biochemistry and Molecular Biology, Michigan State University, East Lansing, MI, USA
6. Department of Medicine, Boston University Medical Center, Boston, MA, USA

*contributed equally to the work

#Corresponding author:
Santhosh Girirajan, MBBS, PhD
205A Life Sciences Building
Pennsylvania State University
University Park, PA 16802
E-mail: sxg47@psu.edu
Phone: 814-865-0674

Keywords: phenotypic variability, modifier, CNV

Abstract

We previously identified a deletion on chromosome 16p12.1 that is mostly inherited and associated with multiple neurodevelopmental outcomes, where severely affected probands carried an excess of rare pathogenic variants compared to mildly affected carrier parents. We hypothesized that the 16p12.1 deletion sensitizes the genome for disease, while "second hits" in the genetic background modulate the phenotypic trajectory. To test this model, we examined how neurodevelopmental defects conferred by knockdown of individual 16p12.1 homologs are modulated by simultaneous knockdown of homologs of "second hit" genes in *Drosophila melanogaster* and *Xenopus laevis*. We observed that knockdown of 16p12.1 homologs affect multiple phenotypic domains, leading to delayed developmental timing, seizure susceptibility, brain alterations, abnormal dendrite and axonal morphology, and cellular proliferation defects. In contrast to genes within the 16p11.2 deletion, which has higher *de novo* occurrence, 16p12.1 homologs additively interacted and were less connected to each other in a human brain-specific interaction network, suggesting that interactions with second-hit genes confer higher impact towards neurodevelopmental phenotypes. Assessment of 358 pairwise interactions in *Drosophila* between 16p12.1 homologs and 76 homologs of patient-specific "second-hit" genes (such as *ARID1B* and *CACNA1A*), genes within neurodevelopmental pathways (such as *PTEN* and *UBE3A*), and transcriptomic targets (such as *DSCAM* and *TRRAP*) identified both additive (47%) and epistatic (53%) effects. In 11 out of 15 families, homologs of patient-specific "second-hits" showed distinct patterns of interactions, enhancing or suppressing the phenotypic effects of one or many 16p12.1 homologs. In fact, homologs of *SETD5* synergistically interacted with homologs of *MOSMO* in both *Drosophila* and *X. laevis*, leading to modified cellular and brain phenotypes, as well as axon outgrowth defects that were not observed with knockdown of either

individual homolog. Our results suggest that several 16p12.1 genes sensitize the genome towards neurodevelopmental defects, and complex interactions with "second-hit" genes determine the ultimate phenotypic manifestation.

Author Summary

Copy-number variants, or deletions and duplications in the genome, are associated with multiple neurodevelopmental disorders. The developmental delay-associated 16p12.1 deletion is mostly inherited, and severely affected children carry an excess of "second-hits" variants compared to mildly affected carrier parents, suggesting that additional variants modulate the clinical manifestation. We studied this "two-hit" model using *Drosophila* and *Xenopus laevis*, and systematically tested how homologs of "second-hit" genes modulate neurodevelopmental defects observed for 16p12.1 homologs. We observed that 16p12.1 homologs independently led to multiple neurodevelopmental features and additively interacted with each other, suggesting that interactions with "second-hit" homologs could have a higher impact towards neurodevelopmental defects than interactions between 16p12.1 homologs. We tested 358 pairwise interactions of 16p12.1 homologs with "second-hit" homologs and genes within conserved neurodevelopmental pathways, and identified interacting homologs in 11 out of 15 families studied, which modified neurodevelopmental defects of individual or multiple 16p12.1 homologs through complex interactions. Interestingly, we observed that *SETD5* homologs interacted with homologs of *MOSMO*, which modified cellular and brain defects, and conferred neuronal phenotypes not observed with knockdown of individual homologs. We propose that the 16p12.1 deletion sensitizes the genome to multiple neurodevelopmental defects, and complex interactions with "second-hit" genes determine the final manifestation.

Introduction

Rare recurrent copy-number variants (CNVs) account for about 15% of individuals with neurodevelopmental disorders, such as autism, intellectual disability, and schizophrenia (1, 2). While certain CNVs were initially associated with specific neuropsychiatric diagnoses, such as the 16p11.2 deletion and autism (3, 4), 3q29 deletion and schizophrenia (5), and 15q13.3 deletion and epilepsy (6), variable expressivity of phenotypes seems to be the norm rather than the exception for these CNVs (7). A notable example of this is the 520 kbp deletion encompassing seven genes on chromosome 16p12.1, which is associated with multiple neuropsychiatric disorders, including intellectual disability/developmental delay (ID/DD), schizophrenia, and epilepsy (8, 9). Furthermore, a large-scale study on a control population reported cognitive defects in seemingly unaffected individuals with the 16p12.1 deletion (10), suggesting that the deletion is sufficient to cause neuropsychiatric features. In contrast to other pathogenic CNVs that occur mostly *de novo*, the 16p12.1 deletion is inherited in more than 95% of individuals from a mildly affected or unaffected carrier parent (8, 9, 11). In fact, affected children with the deletion were more likely to carry another large CNV or deleterious mutation elsewhere in the genome ("second-hit") compared to their carrier parents (8, 9), providing evidence that additional rare variants modulate the effect of the deletion. These results suggest that the 16p12.1 deletion confers significant risk for disease and sensitizes the genome for a range of neuropsychiatric outcomes, while additional rare variants in the genetic background determine the ultimate phenotypic trajectory.

The extensive phenotypic variability and lack of chromosomal events, such as translocations and atypical deletions, have made causal gene discovery for variably-expressive CNVs such as the 16p12.1 deletion challenging. In particular, the developmental and neuronal

103 phenotypes associated with each individual 16p12.1 gene and the interaction models that explain
104 how "second-hit" genes modulate the associated phenotypes have not been assessed. Therefore, a
105 systematic evaluation of developmental, neuronal, and cellular defects caused by reduced
106 expression of individual 16p12.1 genes, as well as their interactions with each other and with
107 "second-hit" genes from patients with the deletion, would allow us to understand the functional
108 basis of the variable phenotypes associated with the deletion. *Drosophila melanogaster* and
109 *Xenopus laevis* serve as excellent models for systematic evaluation of developmental and tissue-
110 specific effects of multiple genes and their genetic interactions, as they are amenable for rapid
111 genetic manipulation and high-throughput evaluation. In fact, *Drosophila* have been classically
112 used to study the roles of genes and genetic interactions towards developmental and neurological
113 phenotypes (12-14). For example, Grossman and colleagues overexpressed human transgenes
114 from chromosome 21 in flies and identified synergistic interactions between *DSCAM* and
115 *COL6A2,* which potentially contribute to the heart defects observed in individuals with Down
116 syndrome (15). Furthermore, functional assays using *X. laevis* have uncovered developmental
117 defects, behaviors, and molecular mechanisms for several homologs of genes associated with
118 neurodevelopmental disorders, such as *NLGN1* (16), *CACNA1C* (17), *GRIK2* (18), and *PTEN*
119 (19).

120 Using *Drosophila* and *X. laevis* models, we recently found that multiple genes within the
121 variably expressive 16p11.2 and 3q29 deletion regions individually contribute to
122 neurodevelopmental defects (20, 21), suggesting that no single gene could be solely causative for
123 the wide range of defects observed with deletion of an entire region. Moreover, we identified
124 complex genetic interactions within conserved biological pathways among homologs of genes
125 affected by these CNVs. For example, fly and *X. laevis* homologs of *NCBP2* enhanced the

126 neuronal and cellular phenotypes of each of the other homologs of 3q29 genes (21), while fly
127 homologs of 16p11.2 genes interacted in cellular proliferation pathways in an epistatic manner to
128 enhance or suppress phenotypes of individual homologs (20). In fact, several aspects of the
129 interactions observed in our studies were also functionally or thematically validated in vertebrate
130 model systems, providing further evidence for the utility of these models to study complex
131 genetic interactions (22, 23). While our previous work showed pervasive interactions of
132 homologs within regions associated with neurodevelopmental disease, the deletions within these
133 regions occur primarily *de novo* (11), indicating a strong phenotypic impact associated with these
134 CNVs. In contrast, the 16p12.1 deletion is mostly inherited and more frequently co-occurs with
135 "second-hit" variants in affected individuals than other pathogenic CNVs (11), suggesting that
136 interactions involving "second-hit" genes confer a higher impact towards the variable
137 neurodevelopmental phenotypes compared to those caused by interactions among genes within
138 the CNV region.

139 Here, using *Drosophila melanogaster* and *X. laevis* as two complementary model systems
140 of development, we present the first systematic assessment of conserved genes within the
141 16p12.1 deletion towards developmental, neuronal, and cellular phenotypes in functional models.
142 We found that knockdown of each individual 16p12.1 homolog affects multiple phenotypic
143 domains of neurodevelopment, leading to developmental delay and seizure susceptibility, brain
144 size alterations, neuronal morphology abnormalities, and cellular proliferation defects. These
145 defects were modulated by simultaneous knockdown of homologs of genes that carried "second-
146 hits" in affected children with the deletion through additive and epistatic interactions. In fact, we
147 observed that knockdown of both fly and *X. laevis* homologs of the intellectual disability-
148 associated gene *SETD5* synergistically enhanced the neurodevelopmental and cellular

149 phenotypes due to knockdown of homologs of the 16p12.1 gene *MOSMO*. Our results suggest a
150 model where reduced expression of each individual gene within 16p12.1 is sufficient to sensitize
151 the genome towards distinct neurodevelopmental defects, and are then modulated by complex
152 interactions with "second-hit" genes.
153
154

155 ## Results

156 **Multiple homologs of 16p12.1 genes contribute to *Drosophila* and *X. laevis* development**

157 We identified four conserved fly homologs out of the seven human protein coding 16p12.1 genes
158 using reciprocal BLAST and orthology prediction tools (S1 Table) (24). Using RNA interference
159 (RNAi) and the *UAS-GAL4* system (25), we reduced the expression of the four fly homologs in a
160 tissue-specific manner, and studied their individual contributions towards developmental,
161 neuronal, and cellular defects (Fig 1). A complete list of the fly lines used in this study and full
162 genotypes for all experiments are provided in S1 File. We confirmed 40-60% expression of the
163 four homologs using RT-qPCR (S1 Fig). We note that the genes are represented with fly gene
164 names along with human counterparts at first mention in the text, and as fly genes with allele
165 names in the figures.

166 We first assessed the global role of 16p12.1 homologs during development by decreasing
167 their expression ubiquitously using the *da-GAL4* driver, and detected larval lethality with
168 knockdown of *Sin* (*POLR3E*) and *UQCR-C2* (*UQCRC2*) (Fig 2A, S2 Fig). Wing-specific
169 bx^{MS1096}*-GAL4* mediated knockdown led to severe phenotypes for *Sin* and severe defects and
170 lethality for *UQCR-C2* fly models, recapitulating the observations made with ubiquitous
171 knockdown (Fig 2A, S2 Fig) and suggesting a role for these homologs in signaling pathways
172 required for early development (26-28). Next, we evaluated whether decreased expression of the
173 homologs leads to neuronal phenotypes frequently observed in animal models of
174 neurodevelopmental disease, including altered lifespan, susceptibility to seizures, delayed
175 developmental timing, changes in brain size, and dendritic arbor defects (29-34). We observed
176 early lethality in adult flies with nervous system-specific *Elav-GAL4*-mediated knockdown of
177 *Sin* and *CG14182* (*MOSMO*) (Fig 2B), while extended lifespan was observed with knockdown of

178 *UQCR-C2*, as previously reported for *Hsp26*, *Hsp27* (35), and *SOD* (36). *UQCR-C2* knockdown
179 in the nervous system also led to significantly greater recovery time when subjected to
180 mechanical stress during bang sensitivity assays, suggesting a higher susceptibility to developing
181 seizures (32) (S2 Fig). Furthermore, evaluation of developmental transitions revealed delayed
182 pupariation and larval lethality with knockdown of *Sin*, indicating a possible role for this gene in
183 developmental timing, as well as partial larval lethality for *CG14182* (Fig 2C). Further, we
184 analyzed neuronal morphology in *Drosophila* class IV sensory neurons using the *ppk-Gal4*
185 driver (31, 37, 38), and identified reduced complexity of dendritic arbors during development for
186 *CG14182* (Fig 2D). Measurements of total area of the developing third instar larval brain led to
187 reduced brain sizes with pan-neuronal knockdown of *CG14182* and *Sin* (Fig 2E, S3 Fig), which
188 corresponded with a decreased number of cells in the brain lobe stained with anti-
189 phosphorylated-Histone 3 (pH3), a marker for proliferating cells (Fig 2F). Interestingly, *Sin*
190 knockdown also led to a reduction in the number of apoptotic cells, as indicated by staining with
191 anti-Death-caspase-1 (Dcp-1) (S3 Fig), likely reflecting its role in both proliferation and
192 apoptotic processes (39, 40).
193 We then performed RNA-sequencing of fly heads with pan-neuronal knockdown of the
194 16p12.1 homologs. Gene Ontology analysis of differentially-expressed genes identified
195 enrichments for multiple cellular, developmental, and neuronal processes (S4 Fig, S2 File). We
196 found that each 16p12.1 homolog disrupted unique sets of biological functions, as 28/52 (53.8%)
197 enriched GO biological process terms were uniquely disrupted by one homolog (S4 Fig).
198 Notably, this trend was accentuated among the human homologs of differentially-expressed
199 genes, with 353/428 (82.5%) GO terms uniquely disrupted by the 16p12.1 homologs, suggesting
200 that they may act within independent pathways (S4 Fig). For example, knockdown of *CG14182*

201 altered the expression of fly homologs of human genes involved in synapse assembly and
202 transmission as well as histone methyltransferase binding function. Similarly, human homologs
203 of genes differentially expressed with knockdown of *Sin* were involved in neuronal projection,
204 neurotransmitter release, and GABA pathways, as well as in the development of several non-
205 neuronal organ systems, including cardiac, kidney, lung, and muscle, further indicating the
206 importance of *Sin* towards global development.

207 Next, we examined developmental phenotypes associated with decreased dosage of
208 homologs of 16p12.1 genes in *X. laevis*, a complementary vertebrate model system (Fig 1 and
209 2G). We injected homolog-specific morpholinos at two- or four-cell stage embryos to reduce the
210 expression of each homolog to approximately 50% (partial knockdown), and further reduced
211 expression with higher morpholino concentrations (stronger knockdown) to increase our
212 sensitivity to detect more specific phenotypes (S1 Fig, see Methods). Reduced expression of
213 *mosmo* and *polr3e* led to severe craniofacial defects in stage 42 tadpoles, as measured by specific
214 facial landmarks, while milder defects were observed for *cdr2* (Fig 2H, S5 Fig). This suggests a
215 role for these homologs in key developmental processes involved in craniofacial morphogenesis,
216 such as neural crest cell formation and migration (41-46). We next examined axon outgrowth
217 phenotypes in neural tube explants from stage 20-22 injected *X. laevis* embryos, and found that
218 stronger knockdown of *mosmo* (20 ng morpholino) led to a significant reduction in axon length
219 (Fig 2I, S5 Fig), suggesting a potential role for the homolog in cytoskeletal signaling processes
220 involved in axon outgrowth (47). Furthermore, stronger knockdown of *mosmo* (20 ng
221 morpholino) and *polr3e* (20 ng morpholino) resulted in decreased forebrain and midbrain area
222 (Fig 2J, S5 Fig), in concordance with the brain size defects we observed in *Drosophila* models.
223 Interestingly, partial knockdown of *mosmo* (12 ng morpholino) also led to a severe reduction in

224 forebrain and midbrain area (Fig S5). Western blot analysis for whole embryo lysates using anti-
225 pH3 antibody as a marker for cellular proliferation showed decreased proliferation with
226 knockdown of *polr3e*, while knockdown of *mosmo* did not lead to any significant changes (S6
227 Fig). Overall, these results suggest that homologs of 16p12.1 genes individually contribute to
228 multiple developmental defects and affect distinct cellular, neuronal and developmental
229 processes in *Drosophila* and *X. laevis*.
230
231 **Homologs of 16p12.1 genes independently contribute to neurodevelopmental defects**
232 Our previous functional studies of genes within CNV regions identified several potential models
233 for how genes within CNVs interact with each other to influence neurodevelopmental
234 phenotypes (20, 21, 48). As multiple homologs of 16p12.1 genes contribute towards
235 developmental, neuronal, and cellular phenotypes, we used the sensitive fly eye system to assess
236 for genetic interactions among the 16p12.1 fly homologs. The *Drosophila* fly eye has been
237 widely used to identify genetic interactions that disrupt ommatidial organization during
238 development (49), and modifier genes for homologs of several human diseases, including
239 Spinocerebellar Ataxia type 1 (50), Huntington's disease (50), and Fragile X syndrome (51),
240 have been studied in flies. We first assessed whether eye-specific *GMR-GAL4* knockdown of
241 individual homologs led to eye phenotypes, and evaluated the severity of eye roughness using
242 *Flynotyper*, a tool that quantifies the levels of ommatidial disorderliness in the adult fly eye (52).
243 We observed that knockdown of *Sin* led to a subtle disruption of ommatidial organization
244 compared with the control, while no such phenotypes were observed with knockdown of the
245 other homologs (S7 Fig). Further reductions in expression of the 16p12.1 homologs using *GMR-*
246 *GAL4* and overexpression of *Dicer2* led to more severe eye phenotypes for *CG14182* and *Sin* (S7

247 Fig). We next generated *GMR-GAL4* eye-specific recombinant lines for each homolog and
248 crossed them with multiple RNAi lines for other 16p12.1 homologs (S1 File), to test a total of 30
249 two-hit crosses for 12 pairwise gene interactions (Fig 1 and 3A, S8 Fig). We observed significant
250 changes in eye severity for a subset of pairwise interactions compared with recombinant lines
251 crossed with control, validated with multiple RNAi lines, and further tested for additive or
252 epistatic effects using two-way ANOVA analysis (53) (Fig 3B and 3C, S9 Fig, see Methods). For
253 example, we observed that simultaneous knockdown of *UQCR-C2* with *Sin* or *CG14182* led to
254 an increase in eye phenotype compared to knockdown of *UQCR-C2* crossed with control (Fig
255 3D). Similarly, decreased expression of *Sin* led to an enhancement of the *CG14182* eye
256 phenotype. Two-way ANOVA analyses indicated that all validated enhancers among the
257 16p12.1 homologs were additive in nature (Fig 3D) (53).

258 We further investigated the effects of the combined knockdown of homologs of *MOSMO*
259 and *POLR3E*, genes that individually contributed to multiple defects in both fly and *X. laevis*
260 models, towards *X. laevis* development (Fig 1 and 3E). Pairwise interactions in *X. laevis* models
261 were tested using partial knockdown of the homologs to avoid potential lethality with stronger
262 knockdown. Partial pairwise knockdown of *polr3e* (10 ng morpholino) and *mosmo* (12 ng
263 morpholino) showed significantly reduced forebrain and midbrain area when compared to
264 knockdown of *polr3e* alone (Fig 3F), but not when compared to knockdown of *mosmo* alone.
265 Similarly, we assessed whether *mosmo* and *polr3e* interact to modulate cellular proliferation
266 processes during *X. laevis* development, and did not observe any changes in anti-pH3 signals
267 with combined knockdown of *polr3e* and *mosmo* compared with knockdown of *polr3e* alone
268 (Fig 3G, S6 Fig). Overall, our analysis in *Drosophila* and *X. laevis* suggest additive effects

269 among the 16p12.1 homologs, where each homolog independently contributes towards the tested
270 neurodevelopmental phenotypes.
271
272 **Homologs of 16p12.1 genes interact with genes in conserved neurodevelopmental pathways**
273 We recently identified additive and epistatic interactions between fly homologs of CNV genes
274 and conserved genes in neurodevelopmental pathways, providing functional evidence that
275 phenotypes of CNV genes are modulated by key neurodevelopmental genes (20, 21). As our
276 functional analyses showed that knockdown of each 16p12.1 homolog resulted in multiple
277 neuronal and developmental phenotypes, we hypothesized that homologs of human genes
278 associated with core neurodevelopmental pathways could modulate these phenotypes (Fig 4A).
279 To examine this, we performed 255 crosses to test 116 pairwise gene interactions between eye-
280 specific recombinant lines for each of the four 16p12.1 homologs and 52 homologs of known
281 neurodevelopmental genes and transcriptional targets. As validation, we used multiple RNAi,
282 mutant or overexpression lines when available, to test a total of 78 fly lines for the 52 homologs
283 (Fig 1). Details of the number of homologs, fly lines, and crosses used for all interaction
284 experiments are provided in S1 File. *First*, we screened for 55 interactions between homologs of
285 16p12.1 genes and 13 homologs of known neurodevelopmental genes, such as *kis (CHD8)*, *Pten*
286 *(PTEN)*, *Ube3a (UBE3A)*, and *Prosap (SHANK3*) (52). Using *Flynotyper* to quantify adult eye
287 defects, we identified global and 16p12.1 homolog-specific interactions for 18 out of 55 tested
288 pairwise interactions (S10-S13 Fig, S3 File). For example, knockdown of *kis* led to a significant
289 reduction in the eye phenotype observed with knockdown of *CG14182* (Fig 4B, S13 Fig).
290 Furthermore, knockdown of *Pten* enhanced the eye phenotype observed with knockdown of *Sin*
291 (S12 Fig), while knockdown of *CG10465 (KCTD13)* enhanced the eye phenotype observed with

292 knockdown of each 16p12.1 homolog (Fig 4B). *Next*, we screened for interactions of the
293 homologs with 25 dysregulated genes selected from our transcriptome studies as well as 14
294 genes within functionally-related pathways, including *NaCP60E (SCN8A)*, *Gat* (*SLC6A1*), and
295 *Hsp70Ab (HSPA1A)*. We identified interactions for 29 out of 61 tested pairs, validated using
296 additional lines when available, including 17 out of 33 interactions of 16p12.1 homologs with
297 their direct transcriptional targets (S3 File). For example, knockdown of *Gat* (*SLC6A1*), *Dscam4*
298 (*DSCAM*), *Nipped-A* (*TRRAP*), and *aurB* (*AURKB*) each modified the eye phenotype due to
299 knockdown of *Sin* (S12 Fig). Furthermore, the protein-folding gene *Hsp23* (*CRYAB)* was
300 upregulated with knockdown of *UQCR-C2* and *Cen*, and overexpression of *Hsp23* enhanced the
301 phenotypes of both 16p12.1 homologs (S10 Fig, S11 Fig). Overall, we identified 47 pairwise
302 interactions between the 16p12.1 homologs and genes from conserved neurodevelopmental
303 pathways, including 25 enhancers and 22 suppressors (S14 Fig, S15 Fig, S3 File), further
304 suggesting a role of these homologs towards neurodevelopment.
305
306 **Homologs of patient-specific "second-hit" genes modulate phenotypes of 16p12.1 homologs**
307 We recently found that an increased burden of rare variants (or "second-hits") outside of disease-
308 associated CNVs, such as 16p11.2 deletion, 15q13.3 deletion, and 16p12.1 deletion, contributed
309 to variability of cognitive and developmental phenotypes among affected children with these
310 CNVs (8, 9, 11). In fact, we found that severely affected children with the 16p12.1 deletion had
311 additional loss-of-function or severe missense variants within functionally intolerant genes
312 compared to their mildly affected carrier parents (8, 9, 11). We hypothesized that homologs of
313 genes carrying patient-specific "second-hits" modulate the effects of individual 16p12.1
314 homologs not only additively but also in an epistatic manner. To test this, we performed 227

315 crosses to study 96 pairwise interactions between eye-specific recombinant lines for each of the
316 four 16p12.1 homologs and 46 RNAi or mutant lines for 24 homologs of patient-specific
317 "second-hit" genes identified in 15 families with the 16p12.1 deletion (Fig 1, S16 Fig, S2 Table)
318 (9). Out of the 24 "second-hit" homologs tested, 12 enhanced and 3 suppressed one or more
319 16p12.1 homologs and confirmed with additional available lines, with a total of 11 out of 15
320 families carrying "second-hit" genes with significant interactions (Fig 4B, S14 Fig, S15 Fig, S3
321 File). Interestingly, we observed that different "second-hit" homologs showed distinct patterns of
322 interactions with homologs of 16p12.1 genes (Fig 4C, S17 Fig). For example, the affected child
323 in family GL_11 carried "second-hit" pathogenic mutations in *NRXN1* and *CEP135*. Knockdown
324 of the fly homolog *Nrx-1* enhanced the eye phenotype caused by knockdown of *Sin* and *UQCR-*
325 *C2*, while knockdown of *Cep135* suppressed the eye phenotype caused by knockdown of *UQCR-*
326 *C2* (Fig 4C). Likewise, the affected child in family GL_01 carried inherited "second-hit" variants
327 in *LAMC3* and *DMD,* as well as a *de novo* loss-of-function mutation in the intellectual disability-
328 associated and chromatin regulator gene *SETD5* (54) (S16 Fig). We found that knockdown of
329 *Lanb2*, homolog of *LAMC3*, and *upSET*, homolog of *SETD5*, led to additive enhancements of the
330 phenotypes caused by knockdown of *UQCR-C2* and *Sin*, respectively (S17 Fig). However,
331 knockdown of *upSET* synergistically enhanced the eye phenotype observed with knockdown of
332 *CG14182* (Fig 5A, S9 Fig). To assess the cellular processes affected by this epistatic interaction
333 during development, we further assessed apoptosis and proliferation processes in the third instar
334 larval eye discs, and found that simultaneous knockdown of *CG14182* and *upSET* led to an
335 increased number of cells undergoing proliferation and apoptosis compared to knockdown of
336 *CG14182* alone (Fig 5B). Interestingly, we also identified epistatic interactions between
337 *CG14182* and other chromatin modifier genes, including *Nipped-A*, a transcriptional target of

338 *Sin*, and *Osa*, homolog of the "second-hit" gene *ARID1B*, identified in family GL_13 (S17 Fig,
339 S3 File). These interactions also modulated cellular proliferation and apoptosis processes in the
340 developing eye discs with knockdown of *CG14182* (S18 Fig).

341 We further evaluated whether interactions between the fly homologs of *POLR3E* and
342 *MOSMO* with *SETD5* were also conserved during vertebrate development, and studied brain and
343 axon outgrowth phenotypes of homologs of these genes in *X. laevis* (Fig 1). We observed that
344 simultaneous knockdown of *polr3e* and *setd5* led to smaller forebrain and midbrain areas
345 compared with *polr3e* knockdown alone (S19 Fig). Similarly, simultaneous knockdown of
346 *mosmo* and *setd5* led to a further reduction in midbrain area than that observed with knockdown
347 of *mosmo* alone (Fig 5C). Furthermore, analysis of axon outgrowth in developing *X. laevis*
348 embryos showed that simultaneous knockdown of *mosmo* and *setd5* led to significantly reduced
349 axon length compared to the individual knockdowns of either *mosmo* or *setd5*, while no changes
350 were observed with simultaneous knockdown of *polr3e* and *setd5* (Fig 5D, S19 Fig). In fact, the
351 axon outgrowth defect observed with simultaneous knockdown of *mosmo* and *setd5* was not
352 observed with partial knockdown of either individual gene. This result mirrors the interactions
353 observed in *Drosophila* eye development, and suggests a synergistic interaction between *mosmo*
354 and *setd5* during nervous system development. Overall, our results show that both additive and
355 epistatic interactions with "second-hit" genes modulate neurodevelopmental and cellular
356 phenotypes associated with homologs of 16p12.1 genes.
357

358 **Discussion**

359 We previously described multiple models for how genes within CNVs contribute towards
360 neurodevelopmental phenotypes (20, 21, 48). Here, we analyzed neurodevelopmental defects and
361 cellular and molecular mechanisms due to individual and pairwise knockdown of conserved
362 16p12.1 homologs in *Drosophila* and *X. laevis*, and evaluated how these defects are modulated
363 by homologs of "second-hit" genes. Our results provide multiple hypotheses for how genes
364 within the deletion contribute to neurodevelopmental phenotypes. *First*, in line with our previous
365 findings for homologs of genes within CNV regions (20, 21), our results show that no single
366 homolog within the 16p12.1 region is solely responsible for the observed neurodevelopmental
367 phenotypes. In fact, we observed a global developmental role for multiple 16p12.1 homologs, as
368 well as specific roles of each homolog towards craniofacial and brain development (S3 Table).
369 The role of 16p12.1 homologs in neurodevelopment was further validated by the interactions we
370 found between the homologs and genes within conserved neurodevelopmental pathways. These
371 findings are in accordance with the core biological functions described for some of these genes.
372 *For example*, *POLR3E* encodes a cofactor of the RNA polymerase III, which is involved in the
373 transcription of small RNA, 5S ribosomal RNA and tRNA (55), while *MOSMO* is a negative
374 regulator of the hedgehog signaling pathway (56). *Second*, knockdown of individual homologs
375 sensitized both model organisms towards specific phenotypes. For example, knockdown of
376 homologs of *MOSMO* led to neuronal morphology defects and knockdown of homologs of
377 *POLR3E* led to brain size phenotypes that correlated with cellular proliferation defects in both
378 model systems, while knockdown of *UQCR-C2* led to seizure susceptibility in flies. *Third*, our
379 interaction studies showed that 16p12.1 homologs additively interact with each other, suggesting
380 their independent contribution towards multiple developmental phenotypes, including eye, brain

381 and cellular proliferation defects. This observation was further supported by distinct sets of
382 biological functions enriched among the differentially expressed genes for each individual
383 knockdown. Beyond the four conserved homologs evaluated in this study, little functional
384 information is available on most of the other genes in the region, including *VWA3A* and *PDZD9*
385 as well as the non-protein coding genes. Results from mouse models of *EEF2K*, which encodes a
386 kinase associated with protein synthesis elongation, have postulated associations of this gene
387 with synaptic plasticity (57), learning and memory (58), atherosclerosis-mediated cardiovascular
388 disease (59), and depression (60). Although *EEF2K* could function in concert with the tested
389 16p12.1 genes to contribute towards neurodevelopmental features, the gene showed low
390 connectivity to other 16p12.1 genes in a human brain-specific interaction network (61, 62) (S4
391 File), providing preliminary evidence that it could also act independently of the other 16p12.1
392 genes. Further functional analyses that includes all protein-coding and non-coding genes are
393 necessary for a comprehensive understanding of the consequences of the entire deleted region, as
394 these genes may also contribute towards the pathogenicity of 16p12.1 deletion.
395 We recently showed that additional variants or "second-hits" modulate the manifestation
396 of developmental and cognitive phenotypes associated with disease-causing variants (8, 9, 11),
397 including intelligence quotient and head circumference phenotypes. Using the 16p12.1 deletion
398 as a paradigm for complex genetics, we examined how homologs of genes carrying "second-hit"
399 variants modulate the phenotypes caused by decreased expression of individual CNV homologs.
400 We observed that knockdown of homologs of genes carrying "second-hits" in severely affected
401 children with the 16p12.1 deletion modified the phenotypes associated with the 16p12.1
402 homologs through complex interactions (15/24 homologs of "second-hits"). In fact, while two-
403 thirds (9/15) of the interacting genes additively modified the phenotypes of the homologs, the

404 remainder of the "second-hit" homologs exhibited epistatic interactions (6/15) with at least one
405 16p12.1 homolog (S3 File). For example, homologs of *ARID1B*, *CEP135* and *CACNA1A*
406 suppressed the eye phenotypes of one or multiple 16p12.1 homologs, while *Dhc98D*, homolog of
407 *DNAH10*, epistatically enhanced the eye phenotype of *UQCR-C2* and *Sin*. Furthermore, we
408 identified a synergistic interaction between homologs of *MOSMO* and *SETD5,* which led to more
409 severe (brain size) and novel (axon outgrowth) neurodevelopmental phenotypes in both
410 *Drosophila* and *X. laevis* compared with knockdown of either individual homolog. Interestingly,
411 mouse embryonic stem cells lacking *Setd5* exhibited dysregulation of genes involved in
412 hedgehog signaling (63), a key pathway recently associated with *MOSMO* function (56).
413 Moreover, we observed that *MOSMO* and *SETD5* are highly connected to each other in a human
414 brain-specific interaction network compared to all genes in the genome (top 84.4 percentile
415 compared to all genetic interactions with *MOSMO*), suggesting that the human genes may also
416 be functionally related (61, 62). We further observed non-additive interactions between
417 *CG14182* and other genes with chromatin regulating function, such as *Nipped-A* (*TRRAP*) and
418 *osa* (*ARID1B*) (S15 Fig). Based on these observations, we propose that while genes carrying
419 "second-hit" variants may additively interact with 16p12.1 genes, they may also synergistically
420 enhance or suppress developmental phenotypes, conferring high impact towards variable
421 neurodevelopmental defects associated with the 16p12.1 deletion. The ultimate nature of these
422 interactions depends on the role of the individual CNV genes towards specific phenotypes, as
423 well as the molecular complexity associated with each phenotypic domain (48).
424 The high inheritance rate of the 16p12.1 deletion (8, 9) suggests that while it confers risk
425 for several phenotypes, the CNV can be transmitted through multiple generations until additional
426 variants accumulate and cumulatively surpass the threshold for severe disease (7). In contrast,

427 other CNVs associated with neurodevelopmental disease, such as the autism-associated 16p11.2
428 deletion and the 17p11.2 deletion that causes Smith-Magenis syndrome, occur mostly *de novo*
429 and are less likely to co-occur with another "second-hit", suggesting a higher pathogenicity on
430 their own (11). For example, 16p11.2 deletion occurs *de novo* in approximately 60% of the
431 cases, and only 8% of the affected children carry another rare large CNV, in contrast to 25% of
432 severely affected children with 16p12.1 deletion that carry a "second-hit" large CNV (11). When
433 we compared experimental results from 16p12.1 homologs with those for fly homologs of
434 16p11.2 genes (20), we found evidence that the differential pathogenicity of the CNVs could be
435 explained by differential connectivity and interactions of genes within each region (Fig 6A) (64).
436 For example, we previously found that 24 out of 52 tested eye-specific interactions between pairs
437 of 16p11.2 homologs led to enhancement or suppression of phenotypes, significantly modifying
438 the effect of the individual genes (Fig 6B) (20). In contrast, only four out of twelve tested
439 interactions between 16p12.1 homologs led to a slight change in phenotypic severity, which in
440 aggregate showed lower phenotypic scores than those observed for pairwise knockdown of
441 16p11.2 homologs (Fig 6B and 6C). Moreover, transcriptome analyses showed a higher overlap
442 of differentially expressed genes among 16p11.2 homologs compared to 16p12.1 homologs,
443 further suggesting a higher functional relatedness among the 16p11.2 genes (Fig 6D). We
444 similarly compared the connectivity of genes within both CNV regions in a human brain-specific
445 interaction network (61, 62), and found that 16p11.2 genes were more strongly connected to each
446 other than were 16p12.1 genes, and were also more strongly connected to each other than with
447 other genes in the genome (Fig 6E and 6F, S20 Fig). Interestingly, genes connecting pairs of
448 16p11.2 genes were enriched for genes intolerant to functional variation (Fig 6E and 6G), such
449 as *ASH1L*, a histone methyltransferase activator and autism candidate gene (65), and *CAMK2B,* a

450 protein kinase gene causative for intellectual disability (66). In contrast, connector genes unique
451 to 16p12.1 genes were not associated with neurodevelopmental disease or enriched for genes
452 intolerant to variation (S4 File). This suggests that the 16p11.2 deletion disrupts a tight network
453 of key genes in the brain, including other neurodevelopmental genes and genes with disease
454 relevance (67, 68). Overall, we propose that 16p12.1 genes independently contribute towards
455 multiple neurodevelopmental phenotypes and exhibit less functional connectivity compared with
456 16p11.2 genes, leading to a high transmissibility of the deletion and higher impact of additional
457 "second-hit" variants towards neurodevelopmental phenotypes.

458 Our study provides the first systematic analysis of individual and pair-wise contributions
459 of 16p12.1 homologs towards basic neurodevelopmental phenotypes and cellular and molecular
460 mechanisms, and identifies a key role of genetic interactions with "second-hit" homologs
461 towards variable developmental phenotypes. Our work does not intend to recapitulate human
462 disease, but rather to highlight the basic cellular roles of individual conserved genes and their
463 interactions towards specific neurodevelopmental phenotypes. As such, these findings should be
464 further examined in higher-order model systems, including mouse and human cellular models.
465 Our functional analyses suggest a model where 16p12.1 genes independently sensitize towards
466 different domains of neurodevelopment, but the ultimate phenotypic manifestation would depend
467 on complex interactions with genes that carry "second-hit" variants in the genetic background.
468 Our results highlight the importance of a thorough functional characterization of both individual
469 CNV genes and their interactions with genes carrying "second-hit" variants towards disease-
470 associated phenotypes.

472 # Materials and Methods

473 **Ethics statement**

474 All *X. laevis* experiments were approved by the Boston College Institutional Animal Care and
475 Use Committee (Protocol #2016–012), and were performed according to national regulatory
476 standards.

477

478 ***Drosophila* stocks and genetics**

479 Using *Ensembl* database (69), NCBI Protein-Protein BLAST tool (70), and DRSC Integrative
480 Ortholog Prediction Tool (DIOPT) (24), we identified four homologs out of the seven genes
481 within the 16p12.1 deletion region in *Drosophila melanogaster* (S1 Table). No fly homologs
482 were present for three genes, including *VWA3A*, *PDZD9* and *EEF2K.* Similar strategies were
483 used to identify fly homologs of conserved neurodevelopmental genes and genes carrying
484 "second-hits" in children with the 16p12.1 deletion. Fly Atlas Anatomy microarray expression
485 data from FlyBase confirmed the expression of each 16p12.1 homolog in the nervous system
486 during *Drosophila* development (S1 Table) (71) and expression data from Xenbase (72)
487 confirmed the expression of the homologs in *X. laevis* brain.

488 Multiple RNAi lines were used to test neurodevelopmental defects of 16p12.1 homologs
489 (S1 File). RNAi, mutant, or overexpression lines for fly homologs were obtained from the
490 Vienna Stock Resource Center (VDRC), Bloomington *Drosophila* Stock Center (BDSC) (NIH
491 P40OD018537), or Kyoto Stock Center (S1 File). The following lines used were generated in
492 various research labs: $Drice^{17_1}$ and $Drice^{17_2}$ from Bergmann lab (73), $GluRIIB^{Overexp\ EGFP}$ from
493 Sigrist lab (74), $Hsp26^{Overexp\ Hsp26}$ from Benzer lab (35), and $Hsp70Ab^{Overexp\ Hsp70\text{-}9.1}$ and
494 $Hsp70Ab^{Overexp\ Hsp70\text{-}4.3}$ from Robertson lab (75). Tissue-specific knockdown of homologs of

495 16p12.1 genes was achieved using the *UAS-GAL4* system (25), with specific *GAL4* lines
496 including w^{1118}*;dCad-GFP, GMR-GAL4/CyO* (Zhi-Chun Lai, Penn State University),
497 w^{1118}*;GMR-GAL4; UAS-Dicer2* (Claire Thomas, Penn State University), w^{1118}*,mcd8-GFP*, *Elav-*
498 *GAL4/Fm7c;; UAS-Dicer2* (Scott Selleck, Penn State University), w^{1118}*,Elav-GAL4* (Mike
499 Groteweil, VCU), w^{1118}*;;Elav-GAL4,UAS-Dicer2* (Scott Selleck, Penn State University),
500 w^{1118}*;da- GAL4* (Scott Selleck, Penn State University), w^{1118}*,*bx^{MS1096}*-GAL4;; UAS-Dicer2* (Zhi-
501 Chun Lai, Penn State University), and *UAS-Dicer2; ppk-GAL4, UAS-mCD8-GFP* (Melissa
502 Rolls, Penn State University). A list of full genotypes for all fly lines and crosses tested in this
503 study is provided in S1 File. Fly crosses were reared on a cornmeal-sucrose-dextrose-yeast
504 medium at room temperature (RT), 25°C or 30°C. For all experiments, RNAi lines were
505 compared to a control with the same genetic background to account for background-specific
506 effects (S1 File). Three different controls were used: w^{1118} from VDRC (GD stock # 60000), in
507 which inverted repeats are inserted by P-element insertion; *y,*w^{1118} from VDRC (KK stock #
508 60100), where inverted repeats are inserted by site-specific recombination; and *{y[1] v[1];*
509 *P{y[+t7.7]=CaryP}*attP2 from BDSC (TRiP stock # 36303).
510

511 **RT-quantitative PCR for *Drosophila* RNAi knockdown of 16p12.1 homologs**

512 Decreased expression of homologs of 16p12.1 genes in the nervous system was confirmed using
513 reverse transcription quantitative PCR (RT-qPCR) for individual *Drosophila* RNAi lines.
514 Decreased expression of the genes was achieved using *Elav-GAL4;;UAS-Dicer2* lines, reared at
515 25°C. As nervous system-specific knockdown of *Sin* with *Elav-GAL4;;UAS-Dicer2* caused
516 developmental lethality in all three RNAi lines tested (Sin^{GD7027}, $Sin^{KK101936}$, $Sin^{HMC03807}$), we
517 confirmed knockdown of *Sin* using *Elav-GAL4* without overexpression of *Dicer2* and reared at

518 RT. We note that all experiments with nervous system-specific knockdown of *Sin* were
519 performed under these conditions. Briefly, three biological replicates, each containing 35-40
520 female heads, were collected after being separated by repeated freezing in liquid nitrogen and
521 vortex cycles. Total RNA was extracted from *Drosophila* heads using TRIzol (Invitrogen,
522 Carlsbad, CA, USA), and cDNA was generated using qScript cDNA synthesis kit (Quantabio,
523 Beverly, MA, USA). Quantitative RT-PCR was performed in an Applied Biosystems Fast 7500
524 system using SYBR Green PCR master mix (Quantabio), with *rp49* as the reference gene.
525 Primers were designed using NCBI Primer-BLAST (76), with primer pairs separated by an
526 intron in the corresponding genomic DNA, if possible. S4 Table details the primers used to
527 quantify the level of expression of 16p12.1 homologs. The delta-delta Ct method was used to
528 calculate the percentage of expression compared to the control (77), and statistical significance
529 compared to the control was determined using t-tests.
530
531 **Eye and wing imaging**
532 Eye-specific knockdown of the 16p12.1 homologs was achieved using *GMR-GAL4* driver at
533 30°C. Female progeny were collected on day 2-3 and imaged using an Olympus BX53
534 compound microscope with LMPLan N 20X air objective and a DP73 c-mount camera at 0.5X
535 magnification, with a z-step size of 12.1µm (Olympus Corporation, Tokyo, Japan). Individual
536 image slices were captured using the CellSens Dimension software (Olympus Corporation,
537 Tokyo, Japan), and were stacked into their maximum projection using Zerene Stacker software
538 (Zerene Systems, Richland, WA, USA). Wing phenotypes were assessed in day 2-5 female
539 progeny from bx^{MS1096}-*GAL4* lines crossed to the RNAi lines at 25°C. Adult wings were imaged
540 using a Zeiss Discovery V20 stereoscope (Zeiss, Thornwood, NY, USA) and a ProgRes Speed

541 XT Core 3 camera (Jenoptik AG, Jena, Germany) with a 40X objective. Adult wing images were
542 captured using ProgRes CapturePro v.2.8.8 software. We characterized qualitative phenotypes
543 for between 10-20 wing images, including curly, wrinkled, shriveled, dusky or vein defects, and
544 10-30 eye images were assessed for rough, glazed, eye size, and necrotic patches defects.
545 Quantitative assessment of rough adult eye phenotypes was performed using a software called
546 *Flynotyper* (20, 52), which calculates a phenotypic score for each eye image by integrating the
547 distances and angles between neighboring ommatidia. The phenotypic scores generated by
548 *Flynotyper* were compared between RNAi lines and their respective controls using one-tailed
549 Mann-Whitney tests, with Benjamini-Hochberg correction for multiple tests.
550
551 **Lifespan Measurement**
552 Lifespan assessment of homologs of 16p12.1 genes was performed as previously reported (78).
553 Briefly, fly crosses were set up at 25°C with *Elav-GAL4;;UAS-Dicer2* for each of the fly
554 homologs, or *Elav-GAL4* at RT for Sin^{GD7027}. In all cases, the newly emerged progeny were
555 collected every day for five consecutive days, and the birth date was recorded. F1 flies were
556 allowed to mate for 24 hours, and were separated under CO_2 into at least four vials, each
557 containing 20 females. Vials were transferred every 2-3 days, and the age and number of living
558 flies were registered. One-way repeated measures ANOVA with post-hoc pairwise t-tests were
559 performed to identify changes in lifespan for the individual 16p12.1 homologs.
560
561 **Bang-sensitive assay**
562 Sensitivity to mechanical stress was assessed in females with decreased expression of 16p12.1
563 homologs in the nervous system, using *Elav-GAL4;;UAS-Dicer2* and reared at 25°C. *Sin* was

564 excluded from the analysis, as adult flies with *Elav-GAL4* knockdown of the gene exhibited
565 severe motor defects. Ten female flies from the progeny were collected on day 0-1 for ten
566 consecutive days, and experiments were performed on day 2-3. Flies were individually separated
567 under CO_2 24 hours before the experiments, collected in culture vials containing food, and
568 transferred to another empty culture vial the day of the experiment. Identification of bang-
569 sensitive phenotypes was performed as previously reported (79). Each vial was vortexed at
570 maximum speed (Fischer Scientific) for 15 seconds, and the time for each fly to recover from
571 paralysis was registered. Differences in bang-sensitivity compared with controls were identified
572 using two-tailed Mann-Whitney tests.
573
574 **Assessment of delay in developmental timing**
575 Pupariation time was assessed in third instar larvae obtained from crosses between RNAi lines
576 and w^{1118}*;;Elav-GAL4,UAS-Dicer2* or w^{1118}*,Elav-GAL4* flies. Developmentally-synced larvae
577 were obtained from apple juice plates with yeast paste, and were reared for 24 hours. Thirty
578 newly emerged first instar larvae were transferred to culture vials, for a total of four to ten vials
579 per RNAi line tested. The number of larvae transitioning to pupae were counted every 24 hours.
580 Significant differences in pupariation timing compared with the control across the duration of the
581 experiment were identified with one-way repeated measures ANOVA and post-hoc pairwise t-
582 tests.
583
584 **Dendritic arborization experiments**
585 Class IV sensory neuron-specific knockdown was achieved by crossing the RNAi lines to *UAS-*
586 *Dicer2; ppk-GAL4* driver at 25°C in apple juice plates. First instar larvae were collected and

587 transferred to cornmeal-based food plates for 48 hours. Z-stack images of the dorsal side of third
588 instar larvae were obtained using a Zeiss LSM 800 (Zeiss, Thornwood, NY, USA) confocal
589 microscope. To perform Sholl analyses, we assessed the number of intersections of dendrite
590 branches with four concentric circles starting from the cell body and separated by 25 μm. The
591 total number of intersections was normalized to the width of the larval hemi-segment, and
592 significant changes compared with control were assessed using two-tailed Mann-Whitney tests.
593

594 **Measurement of larval brain area**

595 Larval brain area was assessed in third instar larvae obtained from crosses between the RNAi
596 lines with *Elav-GAL4*. Crosses were set up in apple plates containing yeast paste to control for
597 size effects generated by food availability. Fifteen first instar larvae were transferred to culture
598 vials containing a fixed volume (8-10 mL) of cornmeal-based food. Brains were dissected from
599 third instar larva in PBS (13mM NaCl, 0.7mM Na_2HPO_4, and 0.3mM NaH_2PO_4), fixed in 4%
600 paraformaldehyde in PBS for 20 minutes, washed three times in PBS, and mounted in Prolong
601 Gold antifade reagent with DAPI (Thermo Fisher Scientific, P36930). Z-stacks of *Drosophila*
602 brains were acquired every 10μm with a 10X air objective with 1.2X magnification using an
603 Olympus Fluoview FV1000 laser scanning confocal microscope (Olympus America, Lake
604 Success, NY). The area of the maximum projection of the Z-stack was measured using Fiji
605 software (80). Differences in brain area were assessed using two-tailed Mann-Whitney tests.
606

607 **RNA sequencing and differential expression analysis in *Drosophila melanogaster***

608 RNA sequencing was performed for three biological replicates of RNA isolated from 35-40
609 *Drosophila* heads with *Elav-GAL4* mediated nervous system-specific knockdown of 16p12.1

610 homologs as well as controls with matching drivers and rearing temperatures. cDNA libraries
611 were prepared with TruSeq Stranded mRNA LT Sample Prep Kit (Illumina, San Diego, CA).
612 Single-end 100bp sequencing of the cDNA libraries was performed using Illumina HiSeq 2000
613 at the Pennsylvania State University Genomics Core Facility, at an average coverage of 35.1
614 million reads/sample. Quality control was performed using Trimmomatic (81), and raw
615 sequencing data was aligned to the fly reference genome and transcriptome build 6.08 using
616 TopHat2 v.2.1.1 (82). Total read counts per gene were calculated using HTSeq-Count v.0.6.1
617 (83). Differences in gene expression were identified using a generalized linear model method in
618 edgeR v.3.20.1 (84), with genes showing a $\log_2$-fold change >1 or < -1 and with a Benjamini-
619 Hochberg corrected FDR<0.05 defined as differentially expressed. Human homologs of
620 differentially-expressed genes in flies were identified using DIOPT v7.0. Biological pathways
621 and processes affected by downregulation of homologs of 16p12.1 genes, defined as significant
622 enrichments of Gene Ontology (GO) terms ($p<0.05$, Fisher's exact test with Benjamini-
623 Hochberg multiple testing correction), were identified using PantherDB (85).
624

625 **Analysis of genetic interactions in the fly eye**

626 To study genetic interactions in the fly eye, we generated recombinant stock lines for each
627 16p12.1 homolog by crossing RNAi lines with eye-specific *GMR-GAL4*, as detailed in S1 File.
628 We assessed genetic interactions between homologs of 16p12.1 genes with each other as well as
629 with homologs of "second-hits" identified in children with the 16p12.1 deletion, conserved
630 neurodevelopmental genes, and select transcriptional targets. Genes carrying "second-hits" were
631 selected as disease-associated genes carrying rare (ExAC frequency ≤1%) copy-number variants,
632 loss-of-function (frameshift, stopgain or splicing) mutations, or *de novo* or likely-pathogenic

633 (Phred-like CADD ≥25) missense mutations previously identified from exome sequencing and
634 SNP microarrays in 15 affected children with the 16p12.1 deletion and their family members (9,
635 86, 87). We also selected conserved genes strongly associated with neurodevelopmental
636 disorders (20, 52) and genes with previously described functional associations with individual
637 16p12.1 genes, such as mitochondrial genes for *UQCRC2* (88) and *Myc* for *POLR3E* and *CDR2*
638 (89, 90). Overall, we tested 212 pairwise gene interactions including 96 interactions with
639 homologs of "second-hit" genes, 55 with neurodevelopmental genes, and 61 with transcriptome
640 targets, using multiple RNAi, mutant or overexpression lines per gene when available.
641 *GMR-GAL4* recombinant lines for the homologs of 16p12.1 genes were crossed with
642 RNAi or mutant lines for the interacting genes to achieve simultaneous knockdown in the eye.
643 We also tested overexpression lines for specific genes that are functionally related to 16p12.1
644 homologs, including *Myc*, *Hsp23*, and *Hsp26*. Our previous assessment showed no changes in
645 phenotypic scores for recombinant lines crossed with *UAS-GFP* compared to crosses with
646 controls, demonstrating that the lines have adequate *GAL4* to bind to two independent *UAS-RNAi*
647 constructs (20). *Flynotyper* scores from flies with double knockdowns were compared to the
648 scores from flies obtained from crosses between 16p12.1 recombinant lines and background-
649 specific controls for the interacting gene. Significant enhancers and suppressors were identified
650 using two-tailed Mann-Whitney tests and Benjamini-Hochberg multiple testing correction. An
651 interaction was considered to be validated when the observed trend was reproduced by multiple
652 RNAi lines when available. Epistatic enhancers were identified as non-additive interactions that
653 showed significant interaction components using two-way ANOVA analysis with multiple
654 testing correction at FDR<0.05 (S9 Fig). When epistatic effects were not confirmed with more
655 than two RNAi lines, if available, the interaction was considered to be additive.

656 **Immunohistochemistry of the developing brain and eye discs in *Drosophila melanogaster***

657 Third instar larvae brain or eye discs were dissected in PBS and fixed in 4% paraformaldehyde in
658 PBT (0.3% Triton X-100 in PBS), followed by three washes with PBT. Preparations were
659 blocked for one hour in blocking buffer (5% FBS or 1% BSA in 0.3% PBT), followed by
660 incubation overnight at 4°C with the primary antibody. We assessed for markers of proliferation
661 using mouse anti-pH3 (S10) (1:100; 9706, Cell Signaling Technology, Danvers, MA, USA) and
662 apoptosis using rabbit anti-Dcp-1 (Asp216) (1:100, 9578, Cell Signaling). Secondary antibody
663 incubation was performed using Alexa fluor 647 goat anti-mouse (1:100, Invitrogen, Carlsbad,
664 CA, USA) and Alexa fluor 568 goat anti-rabbit (1:100, Invitrogen) for 2 hours at 25°C, followed
665 by three washes with PBT. Tissues were mounted in Prolong Gold antifade reagent with DAPI
666 (Thermo Fisher Scientific, P36930) prior to imaging. Z-stacks of brain lobe or eye discs were
667 acquired every 4μm with a 40X air objective with 1.2X magnification using an Olympus
668 Fluoview FV1000 laser scanning confocal microscope (Olympus America, Lake Success, NY).
669 Image analysis was performed using Fiji (80). The number of cells undergoing proliferation or
670 apoptosis were quantified throughout the brain lobe, or posterior to the morphogenetic furrow in
671 the developing eye discs. The total number of Dcp-1 positive cells in larval brain and eye discs,
672 as well as pH3 cells in the eye discs, were manually counted from the maximum projections. The
673 total number of pH3 positive cells in the larval brain were quantified using the MaxEntropy
674 automated thresholding algorithm per slice, followed by counting the number of particles larger
675 than 1.5 μm. Differences in the number of positive pH3 or Dcp-1 cells were compared with
676 appropriate controls using two-tailed Mann-Whitney tests.

677

678 ***Xenopus laevis* embryos**

679 Eggs collected from female *X. laevis* frogs were fertilized *in vitro*, dejellied, and cultured
680 following standard methods (16, 91). Embryos received injections of exogenous mRNAs or
681 antisense oligonucleotide strategies at the two- or four-cell stage, using four total injections
682 performed in 0.1X MMR media containing 5% Ficoll. Embryos were staged according to
683 Nieuwkoop and Faber (92).

684

685 ***X. laevis* gene knockdown and rescue**

686 Morpholinos (MOs) were targeted to early splice sites of *X. laevis mosmo*, *polr3e*, *uqcrc2*, *cdr2*,
687 and *setd5*, or standard control MO (S5 Table), purchased from Gene Tools (Philomath, OR). In
688 knockdown experiments, all MOs were injected at either the 2-cell or 4-cell stage, with embryos
689 receiving injections two or four times total. *mosmo* and control MOs were injected at 12
690 ng/embryo for partial and 20 ng/embryo for stronger knockdown; *polr3e* and control MOs were
691 injected at 10 ng/embryo for partial and 20 ng/embryo for stronger; *uqcrc2* and control MOs
692 were injected at 35 ng/embryo for partial and 50 ng/embryo for stronger; *cdr2* and control MOs
693 were injected at 10 ng/embryo for partial and 20ng for stronger knockdown; and *setd5* and
694 control MOs were injected at 10 ng/embryo for partial knockdown. All double knockdown
695 experiments were performed with partial knockdown to avoid potential lethality.

696 Splice site MOs were validated using Reverse Transcriptase Polymerase Chain Reaction
697 (RT-PCR). Total RNA was extracted using Trizol reagent, followed by chloroform extraction
698 and ethanol precipitation from 2-day old embryos injected with increasing concentrations of MO
699 targeted to each 16p12.1 homolog, respectively. cDNA was synthesized using SuperScript II
700 Reverse Transcriptase (Invitrogen, Carlsbad, CA, USA). PCR was performed in a Mastercycler

701 using HotStarTaq DNA Polymerase (Qiagen, Germantown, MD, USA) following manufacturer
702 instructions. PCR was performed using primers with sequences detailed in S4 Table. RT-PCR
703 was performed in triplicate, and band intensity was measured using the densitometry function in
704 ImageJ (93) and normalized to the uninjected control mean relative to the housekeeping control
705 *odc1*. Phenotypes were rescued with exogenous mRNAs co-injected with their corresponding
706 MO strategies. *X. laevis* ORF for *mosmo* was purchased from the European *Xenopus* Resource
707 Center (EXRC, Portsmouth, UK) and gateway-cloned into pCSF107mT-GATEWAY-3'GFP
708 destination vector. Constructs used were *mosmo*-GFP, and GFP in pCS2+. In rescue
709 experiments, MOs of the same amount used as for the knockdown of each homolog were co-
710 injected along with mRNA (1000pg/embryo for *mosmo*-GFP) in the same injection solution.
711

712 **Quantifying craniofacial shape and size of *X. laevis* embroys**

713 The protocol for quantifying craniofacial shape and size was adapted from Kennedy and
714 Dickinson (94). Embryos at stage 42 were fixed overnight in 4% paraformaldehyde in PBS. A
715 razor blade was used to make a cut bisecting the gut to isolate the head. Isolated heads were
716 mounted in small holes in a clay-lined dish containing PBS. Frontal and lateral view images were
717 taken using a Zeiss AxioCam MRc attached to a Zeiss SteREO Discovery.V8 light microscope
718 (Zeiss, Thornwood, NY, USA). ImageJ software (93) was used to perform craniofacial
719 measurements, including: 1) facial width, which is the distance between the eyes; 2) face height,
720 which is the distance between the top of the eyes and the top of the cement gland at the midline;
721 3) dorsal mouth angle, which is the angle created by drawing lines from the center of one eye, to
722 the dorsal midline of the mouth, to the center of the opposite eye; and 4) midface area, which is
723 the area measured from the top of the eyes to the cement gland encircling the edges of both eyes.

724 For all facial measurements, two-tailed student's t-tests were performed between knockdown
725 embryos and control MO-injected embryos with the same amount of morpholino.
726
727 **Neural tube explants, imaging, and analysis**
728 Embryos were injected with either control MO or 16p12.1 homolog-specific MO at the 2-4 cell
729 stage, and culturing of *Xenopus* embryonic neural tube explants from stage 20-22 embryos were
730 performed as previously described (91). For axon outgrowth analysis, phase contrast images of
731 axons were collected on a Zeiss Axio Observer inverted motorized microscope with a Zeiss
732 20X/0.5 Plan Apo phase objective (Zeiss, Thornwood, NY, USA). Raw images were analyzed by
733 manually tracing the length of individual axons using the NeuronJ plug-in in ImageJ (95). All
734 experiments were performed on multiple independent occasions to ensure reproducibility. Axon
735 outgrowth data were normalized to controls from the same experiment to account for day-to-day
736 fluctuations. Statistical differences were identified between knockdown embryos and control
737 MO-injected embryos with same amounts of morpholino using two-tailed student's t-tests.
738
739 **Immunostaining for brain morphology, imaging, and analysis**
740 For brain morphology analysis, half embryo KDs were performed at the two-cell stage. *X. laevis*
741 embryos were unilaterally injected two times with either control MO or 16p12.1 homolog-
742 specific MO and a GFP mRNA construct (300pg/embryo). The other blastomere was left
743 uninjected. Embryos were raised in 0.1X MMR through neurulation, and then sorted based on
744 left/right fluorescence. Stage 47 embryos were fixed in 4% paraformaldehyde diluted in PBS for
745 one hour, rinsed in PBS, and gutted to reduce autofluorescence. Embryos were processed for
746 immunoreactivity by incubating in 3% bovine serum albumin and 1% Triton-X 100 in PBS for

747 two hours, and then incubated in anti-acetylated tubulin (1:700, T7451SigmaAldrich, St. Louis
748 MO, USA) and goat anti-mouse Alexa Fluor 488 conjugate secondary antibody (1:1000,
749 Invitrogen, Carlsbad, CA, USA). Embryos were rinsed in 1% Tween-20 in PBS and imaged in
750 PBS. Removal of the skin dorsal to the brain was performed if the brain was not clearly visible
751 due to pigment.

752 Images were taken at 3.2X magnification using a Zeiss AxioCam MRc attached to a
753 Zeiss SteREO Discovery.V8 light microscope (Zeiss, Thornwood, NY, USA). Images were
754 processed in ImageJ (93). The areas of the forebrain and midbrain were determined from raw
755 images using the polygon area function in ImageJ. Brain sizes were quantified by taking the ratio
756 of forebrain and midbrain areas between the injected side versus the uninjected side for each
757 sample. All experiments were performed on at least three independent occasions to ensure
758 reproducibility, and data shown represent findings from multiple replicates. Statistical
759 differences were identified between knockdown embryos and control MO injected embryos with
760 the same amount of morpholino using two-tailed student's t-tests.

761

762 **Western blot for cell proliferation**

763 Embryos at stage 20 to 22 were lysed in buffer (50mM Tris pH 7.5, 1% NP40, 150mM NaCl,
764 1mM PMSF, 0.5 mM EDTA), supplemented with cOmplete™ Mini EDTA-free Protease
765 Inhibitor Cocktail (Sigma-Aldrich) and PhosSTOP™ Phosphatase Inhibitor Cocktail (Sigma-
766 Aldrich). Blotting was carried out using rabbit polyclonal antibody to Phospho-Histone H3
767 (Ser10) (1:500, PA5-17869, Invitrogen), with mouse anti-beta actin (1:2500, ab8224, Abcam,
768 Cambridge, MA, USA) as a loading control. Bands were detected by chemiluminescence using
769 Amersham ECL Western blot reagent (GE Healthcare Bio-Sciences, Pittsburgh, PA). Band

770 intensities were quantified by densitometry in ImageJ and normalized to the control mean
771 relative to β-actin.
772
773 **Connectivity of 16p12.1 and 16p11.2 deletion genes in a human brain-specific interaction**
774 **network**
775 We examined the connectivity of human 16p12.1 and 16p11.2 deletion genes in the context of a
776 human brain-specific gene interaction network that was previously built using a Bayesian
777 classifier trained on gene co-expression datasets (61, 62). As the classifier assigned weighted
778 probabilities for interactions between all possible pairs of genes in the genome, we first built a
779 network that only contained the top 0.5% of all pairwise interactions (predicted weights >2.0).
780 Within this network, we identified the shortest paths between each 16p11.2 or 16p12.1 gene and
781 all other protein-coding genes in the genome, using the inverse of the probabilities as weights for
782 each interaction. For each shortest path, we calculated the overall length as a measure of
783 connectivity between the two genes, and also identified the connector genes located within the
784 shortest path. All network analyses were performed using the NetworkX v.2.4 Python package
785 (96). We compared the average connectivity of 16p12.1 genes to 16p11.2 genes, as well as the
786 predicted pathogenicity of connector genes for 16p11.2 and 16p12.1 interactions, using two-
787 tailed Mann-Whitney tests.
788
789 **Statistical analyses**
790 All statistical analyses of functional data were performed using R v.3.4.2 (R Foundation for
791 Statistical Computing, Vienna, Austria). Details for each statistical test, including sample size, p-
792 values with and without multiple testing correction, confidence intervals, test statistics, and
793 ANOVA degrees of freedom, are provided in S5 File.

794 ## Data access

795 Gene expression data for the *Drosophila* RNAi knockdown of homologs of 16p12.1 genes and
796 controls have been submitted to the NCBI Gene Expression Omnibus (GEO;
797 https://www.ncbi.nlm.nih.gov/geo/) under accession number GSE151330, and the raw RNA
798 Sequencing files are deposited in the SRA (Sequence Read Archive) with BioProject database
799 (https://www.ncbi.nlm.nih.gov/bioproject/) accession number PRJNA635495. Source code for
800 the RNA-Sequencing and network analysis is available on the Girirajan lab GitHub page at
801 https://github.com/girirajanlab/16p12_fly_project.
802

803 ## Acknowledgments

804 This work was supported by NIH R01GM121907 and resources from the Huck Institutes of the
805 Life Sciences to S.G, Fulbright Commission Uruguay-ANII to L.P, NIH T32-GM102057 to
806 M.J., and NIH R01GM085115 to M.M.R.
807

808 ## Disclosure declaration

809 Authors disclose no conflict of interest.
810

811 **References**

812 1. Girirajan S, Campbell CD, Eichler EE. Human copy number variation and complex
813 genetic disease. Annu Rev Genet. 2011;45:203-26.
814 2. Wilfert AB, Sulovari A, Turner TN, Coe BP, Eichler EE. Recurrent de novo mutations in
815 neurodevelopmental disorders: properties and clinical implications. Genome Med.
816 2017;9(1):101.
817 3. Weiss LA, Shen Y, Korn JM, Arking DE, Miller DT, Fossdal R, et al. Association
818 between microdeletion and microduplication at 16p11.2 and autism. N Engl J Med.
819 2008;358(7):667-75.
820 4. Zufferey F, Sherr EH, Beckmann ND, Hanson E, Maillard AM, Hippolyte L, et al. A 600
821 kb deletion syndrome at 16p11. 2 leads to energy imbalance and neuropsychiatric disorders.
822 Journal of medical genetics. 2012;49(10):660-8.
823 5. Mulle JG. The 3q29 deletion confers >40-fold increase in risk for schizophrenia. Mol
824 Psychiatry. 2015;20(9):1028-9.
825 6. Helbig I, Mefford HC, Sharp AJ, Guipponi M, Fichera M, Franke A, et al. 15q13.3
826 microdeletions increase risk of idiopathic generalized epilepsy. Nat Genet. 2009;41(2):160-2.
827 7. Girirajan S, Eichler EE. Phenotypic variability and genetic susceptibility to genomic
828 disorders. Human molecular genetics. 2010;19(R2):R176-R87.
829 8. Girirajan S, Rosenfeld JA, Cooper GM, Antonacci F, Siswara P, Itsara A, et al. A
830 recurrent 16p12. 1 microdeletion supports a two-hit model for severe developmental delay.
831 Nature genetics. 2010;42(3):203-9.
832 9. Pizzo L, Jensen M, Polyak A, Rosenfeld JA, Mannik K, Krishnan A, et al. Rare variants
833 in the genetic background modulate cognitive and developmental phenotypes in individuals
834 carrying disease-associated variants. Genet Med. 2018.
835 10. Stefansson H, Meyer-Lindenberg A, Steinberg S, Magnusdottir B, Morgen K,
836 Arnarsdottir S, et al. CNVs conferring risk of autism or schizophrenia affect cognition in
837 controls. Nature. 2014;505(7483):361-6.
838 11. Girirajan S, Rosenfeld JA, Coe BP, Parikh S, Friedman N, Goldstein A, et al. Phenotypic
839 heterogeneity of genomic disorders and rare copy-number variants. New England Journal of
840 Medicine. 2012;367(14):1321-31.
841 12. Gatto CL, Pereira D, Broadie K. GABAergic circuit dysfunction in the Drosophila
842 Fragile X syndrome model. Neurobiol Dis. 2014;65:142-59.
843 13. Jumbo-Lucioni PP, Parkinson WM, Kopke DL, Broadie K. Coordinated movement,
844 neuromuscular synaptogenesis and trans-synaptic signaling defects in Drosophila galactosemia
845 models. Hum Mol Genet. 2016;25(17):3699-714.
846 14. Sears JC, Broadie K. Fragile X Mental Retardation Protein Regulates Activity-Dependent
847 Membrane Trafficking and Trans-Synaptic Signaling Mediating Synaptic Remodeling. Front
848 Mol Neurosci. 2017;10:440.
849 15. Grossman TR, Gamliel A, Wessells RJ, Taghli-Lamallem O, Jepsen K, Ocorr K, et al.
850 Over-expression of DSCAM and COL6A2 cooperatively generates congenital heart defects.
851 PLoS Genet. 2011;7(11):e1002344.
852 16. Chen SX, Tari PK, She K, Haas K. Neurexin-neuroligin cell adhesion complexes
853 contribute to synaptotropic dendritogenesis via growth stabilization mechanisms in vivo. Neuron.
854 2010;67(6):967-83.

855 17. Lewis BB, Wester MR, Miller LE, Nagarkar MD, Johnson MB, Saha MS. Cloning and
856 characterization of voltage-gated calcium channel alpha1 subunits in Xenopus laevis during
857 development. Dev Dyn. 2009;238(11):2891-902.
858 18. Ishimaru H, Kamboj R, Ambrosini A, Henley JM, Soloviev MM, Sudan H, et al. A
859 unitary non-NMDA receptor short subunit from Xenopus: DNA cloning and expression.
860 Receptors Channels. 1996;4(1):31-49.
861 19. Ueno S, Kono R, Iwao Y. PTEN is required for the normal progression of gastrulation by
862 repressing cell proliferation after MBT in Xenopus embryos. Dev Biol. 2006;297(1):274-83.
863 20. Iyer J, Singh MD, Jensen M, Patel P, Pizzo L, Huber E, et al. Pervasive genetic
864 interactions modulate neurodevelopmental defects of the autism-associated 16p11.2 deletion in
865 Drosophila melanogaster. Nat Commun. 2018;9(1):2548.
866 21. Singh MD, Jensen M, Lasser M, Huber E, Yusuff T, Pizzo L, et al. NCBP2 modulates
867 neurodevelopmental defects of the 3q29 deletion in Drosophila and Xenopus laevis models.
868 PLoS Genet. 2020;16(2):e1008590.
869 22. McCammon JM, Blaker-Lee A, Chen X, Sive H. The 16p11.2 homologs fam57ba and
870 doc2a generate certain brain and body phenotypes. Hum Mol Genet. 2017;26(19):3699-712.
871 23. Qiu Y, Arbogast T, Lorenzo SM, Li H, Tang SC, Richardson E, et al. Oligogenic Effects
872 of 16p11.2 Copy-Number Variation on Craniofacial Development. Cell Rep. 2019;28(13):3320-
873 8 e4.
874 24. Hu Y, Flockhart I, Vinayagam A, Bergwitz C, Berger B, Perrimon N, et al. An
875 integrative approach to ortholog prediction for disease-focused and other functional studies.
876 BMC Bioinformatics. 2011;12:357.
877 25. Brand AH, Perrimon N. Targeted gene expression as a means of altering cell fates and
878 generating dominant phenotypes. Development. 1993;118(2):401-15.
879 26. Strigini M, Cohen SM. A Hedgehog activity gradient contributes to AP axial patterning
880 of the Drosophila wing. Development. 1997;124(22):4697-705.
881 27. Yan SJ, Gu Y, Li WX, Fleming RJ. Multiple signaling pathways and a selector protein
882 sequentially regulate Drosophila wing development. Development. 2004;131(2):285-98.
883 28. Yusuff T, Jensen M, Yennawar S, Pizzo L, Karthikeyan S, Gould DJ, et al. Drosophila
884 models of pathogenic copy-number variant genes show global and non-neuronal defects during
885 development. PLoS Genet. 2020;16(6):e1008792.
886 29. Callan MA, Cabernard C, Heck J, Luois S, Doe CQ, Zarnescu DC. Fragile X protein
887 controls neural stem cell proliferation in the Drosophila brain. Hum Mol Genet.
888 2010;19(15):3068-79.
889 30. Kwon CH, Luikart BW, Powell CM, Zhou J, Matheny SA, Zhang W, et al. Pten regulates
890 neuronal arborization and social interaction in mice. Neuron. 2006;50(3):377-88.
891 31. Lee A, Li W, Xu K, Bogert BA, Su K, Gao FB. Control of dendritic development by the
892 Drosophila fragile X-related gene involves the small GTPase Rac1. Development.
893 2003;130(22):5543-52.
894 32. Parker L, Padilla M, Du Y, Dong K, Tanouye MA. Drosophila as a model for epilepsy:
895 bss is a gain-of-function mutation in the para sodium channel gene that leads to seizures.
896 Genetics. 2011;187(2):523-34.
897 33. Rujano MA, Sanchez-Pulido L, Pennetier C, le Dez G, Basto R. The microcephaly
898 protein Asp regulates neuroepithelium morphogenesis by controlling the spatial distribution of
899 myosin II. Nat Cell Biol. 2013;15(11):1294-306.

900 34. Stuss DP, Boyd JD, Levin DB, Delaney KR. MeCP2 mutation results in compartment-
901 specific reductions in dendritic branching and spine density in layer 5 motor cortical neurons of
902 YFP-H mice. PLoS One. 2012;7(3):e31896.
903 35. Wang HD, Kazemi-Esfarjani P, Benzer S. Multiple-stress analysis for isolation of
904 Drosophila longevity genes. Proc Natl Acad Sci U S A. 2004;101(34):12610-5.
905 36. Orr WC, Sohal RS. Extension of life-span by overexpression of superoxide dismutase
906 and catalase in Drosophila melanogaster. Science. 1994;263(5150):1128-30.
907 37. Matthews BJ, Kim ME, Flanagan JJ, Hattori D, Clemens JC, Zipursky SL, et al. Dendrite
908 self-avoidance is controlled by Dscam. Cell. 2007;129(3):593-604.
909 38. Soba P, Zhu S, Emoto K, Younger S, Yang SJ, Yu HH, et al. Drosophila sensory neurons
910 require Dscam for dendritic self-avoidance and proper dendritic field organization. Neuron.
911 2007;54(3):403-16.
912 39. King KL, Cidlowski JA. Cell cycle and apoptosis: common pathways to life and death. J
913 Cell Biochem. 1995;58(2):175-80.
914 40. King KL, Cidlowski JA. Cell cycle regulation and apoptosis. Annu Rev Physiol.
915 1998;60:601-17.
916 41. Hunt P, Gulisano M, Cook M, Sham MH, Faiella A, Wilkinson D, et al. A distinct Hox
917 code for the branchial region of the vertebrate head. Nature. 1991;353(6347):861-4.
918 42. Hunt P, Whiting J, Muchamore I, Marshall H, Krumlauf R. Homeobox genes and models
919 for patterning the hindbrain and branchial arches. Dev Suppl. 1991;1:187-96.
920 43. Lasser M, Pratt B, Monahan C, Kim SW, Lowery LA. The Many Faces of Xenopus:
921 Xenopus laevis as a Model System to Study Wolf-Hirschhorn Syndrome. Front Physiol.
922 2019;10:817.
923 44. Le Lievre CS, Le Douarin NM. Mesenchymal derivatives of the neural crest: analysis of
924 chimaeric quail and chick embryos. J Embryol Exp Morphol. 1975;34(1):125-54.
925 45. Lumsden A, Sprawson N, Graham A. Segmental origin and migration of neural crest
926 cells in the hindbrain region of the chick embryo. Development. 1991;113(4):1281-91.
927 46. Mills A, Bearce E, Cella R, Kim SW, Selig M, Lee S, et al. Wolf-Hirschhorn Syndrome-
928 Associated Genes Are Enriched in Motile Neural Crest Cells and Affect Craniofacial
929 Development in Xenopus laevis. Front Physiol. 2019;10:431.
930 47. Goldberg JL. How does an axon grow? Genes Dev. 2003;17(8):941-58.
931 48. Jensen M, Girirajan S. An interaction-based model for neuropsychiatric features of copy-
932 number variants. PLoS Genet. 2019;15(1):e1007879.
933 49. Thaker HM, Kankel DR. Mosaic analysis gives an estimate of the extent of genomic
934 involvement in the development of the visual system in Drosophila melanogaster. Genetics.
935 1992;131(4):883-94.
936 50. Branco J, Al-Ramahi I, Ukani L, Perez AM, Fernandez-Funez P, Rincon-Limas D, et al.
937 Comparative analysis of genetic modifiers in Drosophila points to common and distinct
938 mechanisms of pathogenesis among polyglutamine diseases. Hum Mol Genet. 2008;17(3):376-
939 90.
940 51. Cziko AM, McCann CT, Howlett IC, Barbee SA, Duncan RP, Luedemann R, et al.
941 Genetic modifiers of dFMR1 encode RNA granule components in Drosophila. Genetics.
942 2009;182(4):1051-60.
943 52. Iyer J, Wang Q, Le T, Pizzo L, Gronke S, Ambegaokar SS, et al. Quantitative
944 Assessment of Eye Phenotypes for Functional Genetic Studies Using Drosophila melanogaster.
945 G3 (Bethesda). 2016;6(5):1427-37.

946 53. Mackay TF. Epistasis and quantitative traits: using model organisms to study gene-gene
947 interactions. Nat Rev Genet. 2014;15(1):22-33.
948 54. Grozeva D, Carss K, Spasic-Boskovic O, Parker MJ, Archer H, Firth HV, et al. De novo
949 loss-of-function mutations in SETD5, encoding a methyltransferase in a 3p25 microdeletion
950 syndrome critical region, cause intellectual disability. Am J Hum Genet. 2014;94(4):618-24.
951 55. Hu P, Wu S, Sun Y, Yuan CC, Kobayashi R, Myers MP, et al. Characterization of human
952 RNA polymerase III identifies orthologues for Saccharomyces cerevisiae RNA polymerase III
953 subunits. Mol Cell Biol. 2002;22(22):8044-55.
954 56. Pusapati GV, Kong JH, Patel BB, Krishnan A, Sagner A, Kinnebrew M, et al. CRISPR
955 Screens Uncover Genes that Regulate Target Cell Sensitivity to the Morphogen Sonic Hedgehog.
956 Dev Cell. 2018;44(2):271.
957 57. McCamphill PK, Farah CA, Anadolu MN, Hoque S, Sossin WS. Bidirectional regulation
958 of eEF2 phosphorylation controls synaptic plasticity by decoding neuronal activity patterns. J
959 Neurosci. 2015;35(10):4403-17.
960 58. Gildish I, Manor D, David O, Sharma V, Williams D, Agarwala U, et al. Impaired
961 associative taste learning and abnormal brain activation in kinase-defective eEF2K mice. Learn
962 Mem. 2012;19(3):116-25.
963 59. Zhang P, Riazy M, Gold M, Tsai SH, McNagny K, Proud C, et al. Impairing eukaryotic
964 elongation factor 2 kinase activity decreases atherosclerotic plaque formation. Can J Cardiol.
965 2014;30(12):1684-8.
966 60. Monteggia LM, Gideons E, Kavalali ET. The role of eukaryotic elongation factor 2
967 kinase in rapid antidepressant action of ketamine. Biol Psychiatry. 2013;73(12):1199-203.
968 61. Greene CS, Krishnan A, Wong AK, Ricciotti E, Zelaya RA, Himmelstein DS, et al.
969 Understanding multicellular function and disease with human tissue-specific networks. Nat
970 Genet. 2015;47(6):569-76.
971 62. Krishnan A, Zhang R, Yao V, Theesfeld CL, Wong AK, Tadych A, et al. Genome-wide
972 prediction and functional characterization of the genetic basis of autism spectrum disorder.
973 Nature neuroscience. 2016;19(11):1454-62.
974 63. Osipovich AB, Gangula R, Vianna PG, Magnuson MA. Setd5 is essential for mammalian
975 development and the co-transcriptional regulation of histone acetylation. Development.
976 2016;143(24):4595-607.
977 64. Andrews T, Honti F, Pfundt R, de Leeuw N, Hehir-Kwa J, Vulto-van Silfhout A, et al.
978 The clustering of functionally related genes contributes to CNV-mediated disease. Genome Res.
979 2015;25(6):802-13.
980 65. Iossifov I, Levy D, Allen J, Ye K, Ronemus M, Lee YH, et al. Low load for disruptive
981 mutations in autism genes and their biased transmission. Proc Natl Acad Sci U S A.
982 2015;112(41):E5600-7.
983 66. Kury S, van Woerden GM, Besnard T, Proietti Onori M, Latypova X, Towne MC, et al.
984 De Novo Mutations in Protein Kinase Genes CAMK2A and CAMK2B Cause Intellectual
985 Disability. Am J Hum Genet. 2017;101(5):768-88.
986 67. Krumm N, Turner TN, Baker C, Vives L, Mohajeri K, Witherspoon K, et al. Excess of
987 rare, inherited truncating mutations in autism. Nature genetics. 2015;47(6):582-8.
988 68. Petrovski S, Wang Q, Heinzen EL, Allen AS, Goldstein DB. Genic intolerance to
989 functional variation and the interpretation of personal genomes. PLoS Genet.
990 2013;9(8):e1003709.

991 69. Yates AD, Achuthan P, Akanni W, Allen J, Allen J, Alvarez-Jarreta J, et al. Ensembl
992 2020. Nucleic Acids Res. 2020;48(D1):D682-D8.
993 70. Altschul SF, Madden TL, Schaffer AA, Zhang J, Zhang Z, Miller W, et al. Gapped
994 BLAST and PSI-BLAST: a new generation of protein database search programs. Nucleic Acids
995 Res. 1997;25(17):3389-402.
996 71. Chintapalli VR, Wang J, Dow JA. Using FlyAtlas to identify better Drosophila
997 melanogaster models of human disease. Nat Genet. 2007;39(6):715-20.
998 72. Bowes JB, Snyder KA, Segerdell E, Jarabek CJ, Azam K, Zorn AM, et al. Xenbase: gene
999 expression and improved integration. Nucleic Acids Res. 2010;38(Database issue):D607-12.
1000 73. Xu D, Wang Y, Willecke R, Chen Z, Ding T, Bergmann A. The effector caspases drICE
1001 and dcp-1 have partially overlapping functions in the apoptotic pathway in Drosophila. Cell
1002 Death Differ. 2006;13(10):1697-706.
1003 74. Schmid A, Hallermann S, Kittel RJ, Khorramshahi O, Frolich AM, Quentin C, et al.
1004 Activity-dependent site-specific changes of glutamate receptor composition in vivo. Nature
1005 neuroscience. 2008;11(6):659-66.
1006 75. Xiao C, Mileva-Seitz V, Seroude L, Robertson RM. Targeting HSP70 to motoneurons
1007 protects locomotor activity from hyperthermia in Drosophila. Dev Neurobiol. 2007;67(4):438-
1008 55.
1009 76. Ye J, Coulouris G, Zaretskaya I, Cutcutache I, Rozen S, Madden TL. Primer-BLAST: a
1010 tool to design target-specific primers for polymerase chain reaction. BMC Bioinformatics.
1011 2012;13:134.
1012 77. Livak KJ, Schmittgen TD. Analysis of relative gene expression data using real-time
1013 quantitative PCR and the 2(-Delta Delta C(T)) Method. Methods. 2001;25(4):402-8.
1014 78. Sun Y, Yolitz J, Wang C, Spangler E, Zhan M, Zou S. Aging studies in Drosophila
1015 melanogaster. Methods Mol Biol. 2013;1048:77-93.
1016 79. Ganetzky B, Wu CF. Indirect Suppression Involving Behavioral Mutants with Altered
1017 Nerve Excitability in DROSOPHILA MELANOGASTER. Genetics. 1982;100(4):597-614.
1018 80. Schindelin J, Arganda-Carreras I, Frise E, Kaynig V, Longair M, Pietzsch T, et al. Fiji: an
1019 open-source platform for biological-image analysis. Nat Methods. 2012;9(7):676-82.
1020 81. Bolger AM, Lohse M, Usadel B. Trimmomatic: a flexible trimmer for Illumina sequence
1021 data. Bioinformatics. 2014;30(15):2114-20.
1022 82. Kim D, Pertea G, Trapnell C, Pimentel H, Kelley R, Salzberg SL. TopHat2: accurate
1023 alignment of transcriptomes in the presence of insertions, deletions and gene fusions. Genome
1024 Biol. 2013;14(4):R36.
1025 83. Anders S, Pyl PT, Huber W. HTSeq--a Python framework to work with high-throughput
1026 sequencing data. Bioinformatics. 2015;31(2):166-9.
1027 84. Robinson MD, McCarthy DJ, Smyth GK. edgeR: a Bioconductor package for differential
1028 expression analysis of digital gene expression data. Bioinformatics. 2010;26(1):139-40.
1029 85. Thomas PD, Campbell MJ, Kejariwal A, Mi H, Karlak B, Daverman R, et al.
1030 PANTHER: a library of protein families and subfamilies indexed by function. Genome Res.
1031 2003;13(9):2129-41.
1032 86. Kircher M, Witten DM, Jain P, O'Roak BJ, Cooper GM, Shendure J. A general
1033 framework for estimating the relative pathogenicity of human genetic variants. Nat Genet.
1034 2014;46(3):310-5.
1035 87. Lek M, Karczewski KJ, Minikel EV, Samocha KE, Banks E, Fennell T, et al. Analysis of
1036 protein-coding genetic variation in 60,706 humans. Nature. 2016;536(7616):285-91.

1037 88. Duncan AM, Ozawa T, Suzuki H, Rozen R. Assignment of the gene for the core protein
1038 II (UQCRC2) subunit of the mitochondrial cytochrome bc1 complex to human chromosome
1039 16p12. Genomics. 1993;18(2):455-6.
1040 89. Gomez-Roman N, Grandori C, Eisenman RN, White RJ. Direct activation of RNA
1041 polymerase III transcription by c-Myc. Nature. 2003;421(6920):290-4.
1042 90. O'Donovan KJ, Diedler J, Couture GC, Fak JJ, Darnell RB. The onconeural antigen cdr2
1043 is a novel APC/C target that acts in mitosis to regulate c-myc target genes in mammalian tumor
1044 cells. PLoS One. 2010;5(4):e10045.
1045 91. Lowery LA, Faris AE, Stout A, Van Vactor D. Neural Explant Cultures from Xenopus
1046 laevis. J Vis Exp. 2012(68):e4232.
1047 92. Nieuwkoop PD FJ. Normal table of Xenopus laevis (Daudin) : a systematical and
1048 chronological
1049 survey of the development from the fertilized egg till the end of metamorphosis: Garland Pub.,
1050 1994; 1994.
1051 93. Schneider CA, Rasband WS, Eliceiri KW. NIH Image to ImageJ: 25 years of image
1052 analysis. Nat Methods. 2012;9(7):671-5.
1053 94. Kennedy AE, Dickinson AJ. Quantitative analysis of orofacial development and median
1054 clefts in Xenopus laevis. Anat Rec (Hoboken). 2014;297(5):834-55.
1055 95. Popko J, Fernandes A, Brites D, Lanier LM. Automated analysis of NeuronJ tracing data.
1056 Cytometry A. 2009;75(4):371-6.
1057 96. Hagberg AA SD, Swart PJ, editor Exploring network structure, dynamics, and function
1058 using NetworkX.
1059 7th Python in Science Conference SciPy 2008; 2008.
1060 97. D'Angelo D, Lebon S, Chen Q, Martin-Brevet S, Snyder LG, Hippolyte L, et al. Defining
1061 the Effect of the 16p11.2 Duplication on Cognition, Behavior, and Medical Comorbidities.
1062 JAMA Psychiatry. 2016;73(1):20-30.
1063 98. Niarchou M, Chawner S, Doherty JL, Maillard AM, Jacquemont S, Chung WK, et al.
1064 Psychiatric disorders in children with 16p11.2 deletion and duplication. Transl Psychiatry.
1065 2019;9(1):8.
1066

1067

1068 ## Figure Legends

1069 **Fig. 1. Strategy to evaluate the individual contributions of homologs of 16p12.1 genes and**
1070 **their interactions with "second-hit" genes towards neurodevelopmental phenotypes. (A)**
1071 Ideogram of human chromosome 16 indicating the deleted region on UCSC genome build
1072 GRCh37, hg19 (chr16:21,948,445-22,430,408) (also known as 16p12.2 deletion). Seven protein
1073 coding genes are located within the 16p12.1 deletion region, including *UQCRC2*, *PDZD9*,
1074 *MOSMO*, *VWA3A*, *EEF2K*, *POLR3E,* and *CDR2*. Four out of the seven genes are conserved in
1075 both *Drosophila melanogaster* and *Xenopus laevis*. **(B)** We performed global and functional
1076 domain-specific phenotypic assessment using RNAi lines and tissue-specific knockdown in
1077 *Drosophila*, and morpholino-mediated whole embryo knockdown in *X. laevis*, to identify
1078 individual contributions of 16p12.1 homologs towards different developmental and neuronal
1079 features. We next evaluated the effect of pairwise knockdown of 16p12.1 homologs towards eye
1080 phenotypes in *Drosophila*, and brain size and cellular proliferation defects in *X. laevis*. We
1081 characterized 212 interactions between the 16p12.1 homologs and homologs of patient-specific
1082 "second-hit" genes identified in children with the deletion, genes within conserved
1083 neurodevelopmental pathways, and differentially-expressed genes identified from RNA-seq
1084 analysis. We found that homologs of "second-hit" genes participate in complex genetic
1085 interactions with 16p12.1 homologs to modulate neurodevelopmental and cellular phenotypes.
1086

1087 **Fig. 2. Multiple homologs of 16p12.1 genes contribute to neurodevelopmental defects in**
1088 ***Drosophila melanogaster* and *X. laevis*.**
1089 **(A)** Schematic showing multiple phenotypes affected by knockdown of individual 16p12.1
1090 homologs in *Drosophila melanogaster*. (**B**) Nervous-system mediated knockdown using *Elav*-

1091 *GAL4* with overexpression of *Dicer2* at 25°C led to reduced lifespan with knockdown of
1092 *CG14182*^{GD2738_2} (n=100, one-way repeat measures ANOVA with post-hoc pairwise t-test, days
1093 6-61, $p<0.05$) and increased lifespan with knockdown of *UQCR-C2*^{GD11238} (n=120, days 51-81,
1094 $p<0.05$). *Elav-GAL4* mediated knockdown of *Sin*^{GD7027} at RT without overexpression of *Dicer2*
1095 led to reduced lifespan of adult flies (n=160, day 1-6, $p<0.05$). Data represented show mean ±
1096 standard deviation of 4-8 independent groups of 20 flies for each line tested. (**C**) Nervous-system
1097 mediated knockdown led to delayed pupariation time and larval lethality for *Sin*^{GD7027} (n=180,
1098 one-way repeat measures ANOVA with post-hoc pairwise t-test, days 6-18, $p<0.05$) and partial
1099 larval lethality for *CG14182*^{GD2738_2} (n=120, days 7-10, $p<0.05$). Data represented show mean ±
1100 standard deviation of 4-9 independent groups of 30 larvae for each line tested. (**D**) Knockdown
1101 of 16p12.1 homologs in sensory class IV dendritic arborization neurons using *ppk-GAL4* with
1102 overexpression of *Dicer2* showed reduced complexity of dendritic arbors (measured as sum of
1103 intersections normalized to width) for *CG14182*^{GD2738} (n=12, two-tailed Mann-Whitney, *p=5.35
1104 $\times 10^{-5}$). Scale bar represents 25 µm. (**E**) Third instar larvae with nervous system-specific
1105 knockdown of 16p12.1 homologs showed reduced brain area for *CG14182*^{GD2738_2} (n=15, two-
1106 tailed Mann-Whitney, *p=0.047) and *Sin*^{GD7027} (n=17, *p= 0.001). (**F**) Developing third instar
1107 larvae with knockdown of *CG14182*^{GD2738_2} (n=15, two-tailed Mann-Whitney, *p=0.026) and
1108 *Sin*^{GD7027} (n=10, *p= 9.74×10^{-4}) showed reduced number of phosphorylated Histone-3 (pH3)
1109 positive cells in the brain lobe (green). Scale bar represents 50 µm. (**G**) Schematic showing the
1110 phenotypes observed with knockdown of 16p12.1 homologs in *X. laevis*. (**H**) Representative
1111 images of tadpoles injected with control morpholino, indicating facial landmarks for face width
1112 (yellow) and orofacial area (red), and tadpoles with knockdown of *polr3e* and *mosmo*.
1113 Knockdown of *cdr2* (n=54, two-tailed student's t-test, *p=7.75 $\times 10^{-4}$), *polr3e* (n=37, *p=1.97

1114 $\times 10^{-13}$) and *mosmo* (n=50, *p=1.36 $\times 10^{-11}$) led to decreased face width, while knockdown of
1115 *polr3e* (*p=3.29 $\times 10^{-16}$) and *mosmo* (*p=1.47 $\times 10^{-8}$) led to decreased orofacial area. All
1116 measures were normalized to their respective control injected with the same morpholino amount.
1117 Scale bar represents 500 µm. (**I**) Strong knockdown of *mosmo* led to decreased axon length in
1118 neural tube explants (n=566, two-tailed student's t-test, *p=7.40 $\times 10^{-12}$). All measures were
1119 normalized to their respective control injected with the same morpholino amount. Representative
1120 schematic for axon length measurements is shown on the left. (**J**) Representative images show
1121 forebrain (red on control image) and midbrain (blue) areas of the side injected with morpholino
1122 (right, red asterisk), which were normalized to the uninjected side (left). Strong knockdown of
1123 *mosmo* (n=67, two-tailed student's t-test, *p<3.07$\times 10^{-13}$) and *polr3e* (n=48, *p<7.39$\times 10^{-4}$) led to
1124 decreased midbrain and forebrain area of *X. laevis* tadpoles (stained with tubulin). Scale bar
1125 represents 500 µm. In all cases, *X. laevis* data represents strong knockdown of the 16p12.1
1126 homologs, except for *cdr2*, which showed lethality and is represented with partial knockdown.
1127 All control data for *X. laevis* represents controls injected with the highest amount of morpholino
1128 (50 ng, see S5 Fig). Boxplots represent all data points with median, 25th and 75th percentiles,
1129 and red dotted lines indicate the control median. Statistical details, including sample size,
1130 confidence intervals and p-values, are provided in S5 File. A list of full genotypes for fly crosses
1131 used in these experiments is provided in S1 File.
1132
1133 **Fig. 3. Homologs of 16p12.1 genes independently contribute towards neurodevelopmental**
1134 **defects.**
1135 (**A**) We generated eye-specific *GMR-GAL4* recombinant lines for the four 16p12.1 homologs to
1136 test a total of twelve pairwise interactions towards eye defects. (**B**) Representative brightfield

1137 images of *Drosophila* adult eyes for recombinant lines of 16p12.1 homologs crossed with RNAi
1138 lines for the other homologs, which show enhancement (Enh.) or suppression (Supp.) of the
1139 phenotypes observed with crosses with control. Scale bar represents 100 µm. (**C**) Simultaneous
1140 knockdown of *UQCR-C2*^{GD11238} with *CG14182*^{GD2738} (n=18, two-tailed Mann-Whitney with
1141 Benjamini-Hochberg correction, *p=0.002) or *Sin*^{GD7027} (n=19, *p=0.023) led to a significant
1142 enhancement in the eye phenotype (measured using *Flynotyper* scores) compared to knockdown
1143 of *UQCR-C2*^{GD11238} alone. Similarly, simultaneous knockdown of *CG14182*^{GD2738} with *Sin*^{GD7027}
1144 (n=19, *p=0.021) enhanced the eye phenotype observed for *CG14182*^{GD2738} alone. Simultaneous
1145 knockdown of *Cen*^{GD9689} with *UQCR-C2*^{GD11238} (n=20, *p=0.023) led to a milder suppression of
1146 the eye phenotype compared to knockdown of *Cen*^{GD9689} alone. Double knockdowns were
1147 compared to the recombinant lines of the 16p12.1 homologs crossed with wild-type controls of
1148 the second 16p12.1 homolog (see S8 Fig). (**D**) Interaction plots for *Flynotyper* scores of pairwise
1149 knockdowns that led to a significant enhancement of the eye phenotype of individual 16p12.1
1150 homologs. The interaction plots show changes in *Flynotyper* scores (mean ± s.d.) for *GMR-*
1151 *GAL4* control (grey) or *CG14182*^{GD2738} (blue) and *UQCR-C2*^{GD11238} (green) recombinant lines
1152 crossed with either wild-type control (left) or with *Sin*^{GD7027} and *CG14182*^{GD2738_2} as "second
1153 hits" (right). Two-way ANOVA tests showed no epistatic effects for the interactions (p>0.05),
1154 suggesting additive effects of the homologs towards eye phenotypes. (**E**) We generated double
1155 knockdowns of 16p12.1 homologs in *X. laevis* models by co-injecting embryos with morpholinos
1156 of two homologs. All double knockdown experiments were performed with partial knockdown
1157 of the genes, to avoid potential lethality with stronger knockdown. (**F**) Representative images of
1158 tadpoles stained with anti-tubulin show forebrain (red on control image) and midbrain (blue)
1159 areas of the side injected with morpholino (right, red asterisk), which were normalized to the

1160 uninjected side (left). Simultaneous knockdown of *polr3e* and *mosmo* led to decreased forebrain
1161 (n=36, two-tailed student's t-test, *$p=1.10\times10^{-9}$) and midbrain area (*$p=1.98\times10^{-7}$), which
1162 showed no differences compared to partial knockdown of *mosmo* alone. Control data represents
1163 control injected with highest amount of morpholino (22ng). Scale bar represents 500 μm. (**G**)
1164 Representative western blots show bands for phosphorylated histone-3 (pH3) and β-actin for the
1165 uninjected control, knockdown of *polr3e*, knockdown of *mosmo*, and pairwise knockdown of
1166 *polr3e* and *mosmo* (full western blots are shown in S6 Fig). Bar plot shows intensity of pH3 band
1167 normalized to β-actin. Simultaneous knockdown of *polr3e* and *mosmo* does not lead to changes
1168 in the proliferation defects observed with knockdown with *polr3e* alone. Boxplots represent all
1169 data points with median, 25th and 75th percentiles, and red dotted lines indicate the control
1170 median. Statistical details, including sample size, confidence intervals and p-values, are provided
1171 in S5 File. A list of full genotypes for fly crosses used in these experiments is provided in S1
1172 File.
1173
1174 **Fig. 4. Homologs of 16p12.1 genes show complex interactions with homologs of patient-**
1175 **specific "second-hit" and conserved neurodevelopmental genes.**
1176 **(A)** We evaluated how homologs of genes outside of the CNV region (*Gene B*), including genes
1177 carrying "second-hit" variants in children with the 16p12.1 deletion, genes within conserved
1178 neurodevelopmental pathways, and transcriptome targets, affect the phenotypes observed for
1179 homologs of 16p12.1 genes. We crossed eye-specific recombinant lines for each homolog with a
1180 total of 124 RNAi, mutant or overexpression lines for 76 interacting genes to test a total of 212
1181 pairwise gene combinations. (**B**) Heatmaps show the fold-change (FC) of *Flynotyper* scores for
1182 pairwise interactions of 16p12.1 homologs with select lines of interacting homologs, compared

1183 to recombinant lines for the homologs crossed with control. Grey boxes indicate pairwise crosses
1184 that were not tested or were not validated by multiple lines. (**C**) Representative pedigrees of
1185 families with 16p12.1 deletion (affected child in black, carrier parent in grey) that were selected
1186 to study the effect of homologs (represented within parenthesis) of genes carrying "second-hits"
1187 towards phenotypes of homologs of 16p12.1 genes. Interaction plots and representative
1188 brightfield adult eye images for validated enhancers (Enh.) or suppressors (Supp.) are shown
1189 below each pedigree. Interaction plots show the changes in *Flynotyper* scores (mean ± s.d.) for
1190 *GMR-GAL4* control (grey) or recombinant lines of 16p12.1 homologs crossed with either wild-
1191 type control line (left) or with "second-hit" homologs (right). Two-way ANOVA analyses
1192 showed epistatic enhancements for $CG14182^{GD2738}/upSET^{HMC03177}$, $Sin^{GD7027}/Dhc98D^{MB03402}$, and
1193 $UQCR\text{-}C2^{GD11238}/Dhc98D^{MB03402}$ ($p<0.05$ with Benjamini-Hochberg correction), while
1194 $Cep135^{GD5121_2}$ suppressed $UQCR\text{-}C2^{GD11238}$. Scale bar represents 100 μm. Details of number of
1195 homologs, fly lines and crosses, as well as a list of full genotypes for all interaction experiments
1196 are provided in S1 File. Statistical details, including sample size, confidence intervals and p-
1197 values, are provided in S5 File.
1198
1199 **Fig. 5. Homologs of *SETD5* synergistically interact with homologs of *MOSMO* to modify**
1200 **neurodevelopmental defects.**
1201 (**A**) Pedigree of a family with 16p12.1 deletion, with the proband also carrying a *de novo*
1202 pathogenic mutation in *SETD5*. Interaction plot and representative brightfield adult eye images
1203 for control, *GMR-GAL4* knockdown of $CG14182^{GD2738}$, $upSET^{HMC03177}$ and
1204 $CG14182^{GD2738}/upSET^{HMC03177}$ show a synergistic enhancement with simultaneous knockdown of
1205 the homologs. Interaction plots show changes in *Flynotyper* scores (mean ± s.d.) for *GMR-GAL4*

1206 control (grey) or recombinant lines of *CG14182*^{GD2738} and *Sin*^{GD7027} crossed with either wild-type
1207 control line (left) or with *upSET*^{HMC03177} (right). (**B**) Representative confocal images of third
1208 instar larval eye discs stained with anti-phosphorylated histone-3 (pH3, green) or anti-Dcp-1
1209 (red), markers of cellular proliferation and apoptosis, respectively. Positive pH3 or Dcp-1 cells
1210 were quantified posterior to the morphogenetic furrow, indicated by white boxes in left panels.
1211 Double knockdown of *CG14182*^{GD2738}/*upSET*^{HMC03177} led to increased pH3 (n=17, two-tailed
1212 Mann-Whitney, *p= 0.046) and Dcp-1 (n=19, *p=0.006) positive cells compared to knockdown
1213 of *CG14182*^{GD2738} alone. The double knockdown also led to increased Dcp-1 positive cells
1214 compared to knockdown of *upSET*^{HMC03177} alone (*p= 2.19×10^{5}). Scale bar represents 50 µm.
1215 (**C**) Representative images of tadpoles stained with anti-tubulin show forebrain (red on control
1216 image) and midbrain (blue) areas of the side injected with morpholino (right, red asterisk), which
1217 were normalized to the uninjected side (left). Partial knockdown of *mosmo* with *setd5* led to a
1218 reduction in the midbrain area compared to the knockdown of *mosmo* alone (n=16, two-tailed
1219 student's t-test, *p= 0.047). Control data represents control injected with highest amount of
1220 morpholino (22ng). Scale bar represents 500 µm (**D**) Normalized axon length of *X. laevis*
1221 tadpoles with simultaneous knockdown of *mosmo* and *setd5* led to a significant reduction in axon
1222 length that was not observed with partial knockdown of *mosmo* (n=438, two-tailed student's t-
1223 test, *p= 3.34×10^{-6}) or *setd5* (*p=1.86×10^{-9}). All measures were normalized to their respective
1224 controls injected with the same morpholino amount (See S19 Fig). Control data represents
1225 controls injected with highest amount of morpholino (22ng). All double knockdown experiments
1226 were performed with partial knockdown of the genes, to avoid potential lethality with stronger
1227 knockdown. Boxplots represent all data points with median, 25th and 75th percentiles, and red
1228 dotted lines indicate the control median. A list of full genotypes for fly crosses used in these

1229 experiments is provided in S1 File. Statistical details, including sample size, confidence intervals
1230 and p-values, are provided in S5 File.
1231
1232 **Fig. 6. Functional relatedness of genes within disease-associated CNV regions correlate**
1233 **with higher pathogenicity.**
1234 (**A**) Bar plot shows frequency of reported *de novo* occurrence of the 16p12.1 deletion (9, 11)
1235 compared to the autism-associated 16p11.2 deletion (11, 97, 98). Schematic shows our model for
1236 higher functional connectivity of genes within the 16p11.2 region compared to the 16p12.1
1237 region. Only genes with *Drosophila* homologs are represented. (**B**) Pairwise eye-specific
1238 knockdown of 16p11.2 homologs (*rl*, *CG10465* and *Pp4-19C* crossed with other 16p11.2
1239 homologs) lead to more severe phenotypic scores compared to pairwise interactions of 16p12.1
1240 homologs (n=36 for 16p11.2, n=12 for 16p12.1, one-tailed Mann-Whitney, *$p=3.51 \times 10^{-5}$). Grey
1241 circles represent pairwise interactions, while 16p11.2 and 16p12.1 single-homolog knockdowns
1242 are represented in orange and green, respectively. (**C**) Phenotypic scores of individual 16p11.2
1243 homologs (grey) are significantly enhanced or suppressed by a second 16p11.2 homolog
1244 (orange). In contrast, little variation in phenotypic scores is observed for 16p12.1 homologs
1245 (grey) with simultaneous knockdown of another homolog (green). The interacting homologs are
1246 labeled as follows: A: *Pp4-19C* (*PPP4C*), B: *CG17841* (*FAM57B*), C: *coro* (*CORO1A*), D: *Ald1*
1247 (*ALDOA*), E: *Rph* (*DOC2A*), F: *Tao* (*TAOK2*), G: *Asph* (*ASPHD1*), H: *klp68D* (*KIF22*), I: *Pa1*
1248 (*PAGR1*), J: *Pis* (*CDIPT*), K: *CG10465* (*KCTD13*), L: *CG15309* (*YPEL3*), M: *Doc3*, (*TBX6*), N:
1249 *rl* (*MAPK3*), W: *CG14182* (*MOSMO*), X: *Cen* (*CDR2*), Y: *Sin* (*POLR3E*), Z: *UQCR-C2*
1250 (*UQCRC2*). (**D**) Pairs of 16p11.2 homologs exhibit a higher proportion of shared differentially-
1251 expressed genes compared to pairs of 16p12.1 homologs (n=30 for 16p11.2, n=12 for 16p12.1,

1252 two-tailed Mann-Whitney test, *p= 0.031). (**E**) Network diagram shows connections between
1253 human 16p11.2 or 16p12.1 genes within a brain-specific interaction network. 16p12.1 genes are
1254 indicated in green, 16p11.2 genes in orange, connector genes in grey, and connector genes that
1255 are intolerant to functional variation (RVIS $\leq$ 20th percentile) in dark green. *C16orf92* and
1256 *C16orf54* for 16p11.2 and *PDZD9* for 16p12.1 were not present in the brain network and were
1257 therefore excluded from the network analysis. (**F**) Genes within the 16p11.2 region show higher
1258 average pairwise connectivity in a human brain-specific network, measured as the inverse of the
1259 shortest paths between two genes, compared to 16p12.1 genes (n=25 for 16p11.2, n=6 for
1260 16p12.1, two-tailed Mann-Whitney, *p=0.036, see S4 File). (**G**) 16p11.2 connector genes have
1261 lower RVIS percentile scores compared to 16p12.1 connector genes (n=166 for 16p11.2, n=33
1262 for 16p12.1, two-tailed Mann-Whitney, *p=0.017, see S4 File). Functionally-intolerant genes are
1263 represented in dark green. Boxplots represent all data points with median, 25th and 75th
1264 percentiles. Statistical details are provided in S5 File.
1265

1266 ## Supporting Information Legends

1267 **S1 Fig. Expression levels of 16p12.1 homologs in *Drosophila* and *X. laevis*.**

1268 **(A)** *Drosophila* homologs of 16p12.1 genes were knocked down using nervous system-specific
1269 *Elav-GAL4* driver with overexpression of *Dicer2* at 25°C. RT-qPCR confirmed 40-60%
1270 knockdown of the 16p12.1 homologs (two-tailed student's t-test, *p<0.05). As knockdown of *Sin*
1271 caused embryonic lethality in these conditions, all experiments in the nervous system and RT-
1272 qPCR were performed without overexpression of *Dicer2* and reared at room temperature (RT).
1273 $Sin^{KK101936}$ and $Sin^{HMC03807}$ were also embryonic lethal without *Dicer2*. Sin^{GD7027_2} did not show
1274 knockdown of the homolog, and the RNAi line was therefore not used for further experiments. A
1275 list of full genotypes for fly crosses used in these experiments is provided in S1 File. (**B)**
1276 Normalized band intensity of RT-PCR of *X. laevis* tadpoles injected with different morpholino
1277 dosages of the 16p12.1 homologs compared to the uninjected control. Different morpholino
1278 sequences were used for the L and S alleles for *uqcrc2* and *mosmo*, while unique sequences were
1279 used for both L and S alleles for *cdr2* or *setd5*. As the S allele has not been annotated for *polr3e*,
1280 only the L allele was targeted. Colored bars represent the dosages of morpholinos used, with
1281 grey bars indicating amounts for "partial knockdown" (approximately 50% of expression) and
1282 black bars indicating amounts for "stronger knockdown". 10ng of morpholino was used for
1283 partial and stronger KD experiments for *mosmo* S allele, as increasing concentrations did not
1284 lead to differences in knockdown of the allele. Bar plots represent mean +/- SD, and red dotted
1285 lines indicate 50% expression. Statistical details are provided in S5 File.

1286

1287 **S2 Fig. Global neurodevelopmental defects with knockdown of 16p12.1 *Drosophila***
1288 **homologs.**

1289 (**A**) Summary of phenotypes observed with tissue-specific knockdown of each of the 16p12.1
1290 homologs. (**B)** Ubiquitous (*Da-GAL4*) and nervous system-specific (*Elav-GAL4*) knockdown of
1291 multiple RNAi lines for each 16p12.1 homolog showed a range of lethality and developmental
1292 defects. (**C**) Representative brightfield images of adult wings with knockdown of 16p12.1
1293 homologs using the wing-specific driver bx^{MS1096}-*GAL4*. Severe phenotypes were observed for
1294 *UQCR-C2* and *Sin*, with some RNAi lines, including $UQCR\text{-}C2^{GD11238_2}$, $UQCR\text{-}C2^{KK108812}$ and
1295 Sin^{GD7027}, showing lethality. Scale bar represents 500µm. (**D)** Bang sensitivity assay for adult
1296 flies with nervous system-specific knockdown of the 16p12.1 homologs showed increased
1297 recovery time for $UQCR\text{-}C2^{GD11238}$ (n=95, two-tailed Mann-Whitney test, *p=0.003). Sin^{GD7027}
1298 adult flies exhibited severe motor defects and could not be tested for the phenotype. Boxplots
1299 represent all data points with median, 25th and 75th percentiles. Statistical details are provided in
1300 S5 File. A list of full genotypes for fly crosses used in these experiments is provided in S1 File.
1301

1302 **S3 Fig. Sin^{GD7027} and $CG14182^{GD2738_2}$ lead to decreased brain area and decreased number**
1303 **of proliferating cells in the brain.**

1304 (**A**) Representative confocal brightfield images of nervous system-specific knockdown of
1305 16p12.1 homologs show decreased total brain area for Sin^{GD7027} and $CG14182^{GD2738_2}$. Scale bars
1306 represent 100µm. (**B**) *Elav-GAL4* mediated knockdown led to decreased number of
1307 phosphorylated histone-3 positive cells (pH3, green) in the brain lobe (DAPI, blue) with
1308 knockdown of Sin^{GD7027} (n=10, two-tailed Mann-Whitney, *p= 9.74×10^{-4}) and $CG14182^{GD2738_2}$
1309 (n=15, *p=0.026), indicating decreased proliferation with knockdown of the homologs.
1310 Knockdown of Sin^{GD7027} led to decreased number of Dcp-1 positive cells (*p= 2.78×10^{-4}, red) in
1311 the brain lobe. Scale bar represents 50µm. Boxplots represent all data points with median, 25th

1312 and 75th percentiles. Statistical details, including sample size, confidence intervals and p-values,
1313 are provided in S5 File. A list of full genotypes for fly crosses used in these experiments is
1314 provided in S1 File.
1315
1316 **S4 Fig. Enriched GO terms observed with knockdown of 16p12.1 fly homologs in the**
1317 **nervous system.**
1318 (**A**) Clusters of enriched Gene Ontology (GO) Biological Process terms for differentially
1319 expressed fly genes observed with nervous system-specific knockdown of 16p12.1 homologs
1320 (left) and their human homologs (right). While some clusters of terms overlap among 16p12.1
1321 homologs, genes dysregulated with knockdown of individual homologs exhibit unique
1322 enrichments for GO terms, suggesting their independent action towards neuronal development.
1323 Venn diagrams show overlaps of enriched GO Complete Biological Processes terms for (**B**)
1324 differentially-expressed fly genes observed with knockdown of individual 16p12.1 homologs, or
1325 (**C**) human homologs of the fly genes. A list of differentially expressed genes with knockdown of
1326 16p12.1 homologs, as well as a list of all enriched GO terms for these gene sets, is detailed in S2
1327 File. Venn diagrams were constructed using Venny 2.1 software (https://bioinfogp.cnb.csic.es/
1328 tools/venny).
1329
1330 **S5 Fig. Decreased dosage of 16p12.1 homologs leads to multiple neurodevelopmental**
1331 **phenotypes in *X. laevis*.**
1332 **(A)** Representative images of tadpoles injected with control morpholino or morpholinos for
1333 16p12.1 homologs, indicating facial landmarks for face width (yellow), height (blue), angle
1334 (green), and orofacial (red) and eye (orange) area. Boxplots showing face height, width, angle,

1335 and orofacial and eye area of each knockdown compared to its own control. Knockdown of
1336 *mosmo* (n=50, two-tailed student's t-test, *p=0.010) and *cdr2* (n=54, *p=3.68×10^{-6}) led to
1337 increased face height. Knockdown of *cdr2* (*p=7.75×10^{-4}), *polr3e* (n=37, *p=1.97×10^{-13}) and
1338 *mosmo* (*p=1.36×10^{-11}) led to decreased face width, while knockdown of *cdr2* (*p= 1.03×10^{-8}),
1339 *polr3e* (*p= 2.73×10^{-4}) and *mosmo* (*p= 3.50×10^{-7}) led to decreased face angle. Knockdown of
1340 *polr3e* (*p=3.29×10^{-16}) and *mosmo* (*p=1.47×10^{-8}) led to decreased orofacial area, and
1341 knockdown of *polr3e* (*p=1.01×10^{-18}), *mosmo* (*p= 7.23×10^{-10}) and *cdr2* (*p= 0.009) led to
1342 decreased eye area. Data represents strong knockdown of the 16p12.1 homologs, except for *cdr2*,
1343 which showed lethality and is represented with partial knockdown. All measures were
1344 normalized to their respective control injected with the same morpholino amount. Scale bars
1345 represent 500µm. **(B)** Boxplots showing axon length of each knockdown compared to its own
1346 control. Strong knockdown of *mosmo* led to decreased axon length in neural tube explants
1347 (n=548, two-tailed student's t-test, *p=7.40×10^{-12}), which was rescued by co-injection with
1348 overexpressed (OE) mRNA of the gene (n=566, *p= 4.06×10^{-5}). All measures were normalized
1349 to their respective control injected with the same morpholino amount. (**C**) Representative images
1350 stained with anti-tubulin show forebrain (red on control image) and midbrain (blue) areas of the
1351 side injected with morpholino (right, red asterisk), which were normalized to the uninjected side
1352 (left). Partial knockdown of *mosmo* led to decreased forebrain (n=47, two tailed student's t-test,
1353 *p= 1.18×10^{-9}) and midbrain (*p=1.45×10^{-7}) area. Graphs represent contralateral ratio of brain
1354 area compared to uninjected side of the embryo. Scale bars represent 500µm. All boxplots
1355 represent all data points with median, 25th and 75th percentiles. In each case, measurements for
1356 each knockdown were compared to controls injected with equal amounts of morpholino.

1357 Statistical details, including sample size, confidence intervals and p-values, are provided in S5
1358 File.
1359
1360 **S6 Fig. Whole western blot for phosphorylated histone-3 in *X. laevis* embryos with**
1361 **knockdown of *polr3e*, *mosmo* and *setd5*.**
1362 (**A**) Three replicate western blot experiments were performed. The intensity of bands at 17 kDa,
1363 corresponding with pH3 (top, indicated with arrow), were normalized to the β-actin loading
1364 control (bottom). (**B**) Partial knockdown of *polr3e* shows reduced band intensity with anti-pH3
1365 antibody compared to β-actin loading control. Bar plot represents mean ± SD.
1366
1367 **S7 Fig. Knockdown of *Sin* and *CG14182* lead to disruption of the fly eye in a dosage**
1368 **sensitive manner.**
1369 (**A**) Representative brightfield adult eye images and *Flynotyper* phenotypic scores of eye-specific
1370 knockdown of 16p12.1 homologs with *GMR-GAL4* and no overexpression of *Dicer2* at 30°C. A
1371 mild eye phenotype was observed with knockdown of *Sin*, replicated across multiple RNAi lines
1372 (two-tailed Mann-Whitney with Benjamini-Hochberg correction, *$p<0.05$). (**B**) Representative
1373 images and *Flynotyper* scores of eye-specific knockdown of 16p12.1 homologs with *GMR-GAL4*
1374 and overexpression of *Dicer2* at 30°C. Severe eye phenotypes were observed for all tested RNAi
1375 lines of *Sin* (*$p< 1.13\times10^{-4}$) and *CG14182* (*$p< 4.70\times10^{-4}$). Scale bar represents 100 μm.
1376 Boxplots represent all data points with median, 25th and 75th percentiles, and red dotted lines
1377 indicate the control median. Statistical details, including sample size, confidence intervals and p-
1378 values, are provided in S5 File. A list of full genotypes for fly crosses used in these experiments
1379 is provided in S1 File.

1380

1381 **S8 Fig. Pairwise knockdown of homologs of 16p12.1 genes lead to moderate changes in eye**

1382 **severity compared to individual knockdown of genes.**

1383 (**A-D**) Pairwise knockdown of homologs of 16p12.1 genes led to subtle changes in phenotypic

1384 scores, with only four significant interactions (compared to control lines) validated by multiple

1385 RNAi lines. *Sin* and *CG14182* enhanced the eye phenotype of *UQCR-C2*^{GD11238}, while *Sin*

1386 enhanced *CG14182*^{GD2738} eye phenotype and *UQCR-C2* suppressed *Cen*^{GD9689} eye phenotype

1387 (two-tailed Mann-Whitney with Benjamini-Hochberg correction, *$p<0.05$). Boxplots represent

1388 all data points with median, 25th and 75th percentiles. Red dotted lines indicate the median of

1389 recombinant lines crossed with control. Statistical details, including sample size, confidence

1390 intervals and p-values, are provided in S5 File. A list of full genotypes for fly crosses used in

1391 these experiments is provided in S1 File.

1392

1393

1394 **S9 Fig. Definition of genetic interactions of 16p12.1 homologs towards eye phenotypes used**

1395 **in this study.**

1396 We defined enhancers as additive or epistatic by comparing phenotypic scores of two-hit

1397 experiments using two-way ANOVA. The phenotypic scores of flies obtained from crosses of

1398 *GMR-GAL4* lines or 16p12.1 recombinant lines with controls (left) were compared to their

1399 respective crosses with the "second-hit" RNAi line (right, "*Gene B*"). The magnitude of change

1400 in phenotypic scores between experiments involving "second-hits" versus controls was not

1401 different ($p>0.05$) between crosses of recombinant lines compared to those of *GMR-GAL4* for

1402 additive interactions. The magnitude of change was significantly different ($p<0.05$ with

1403 Benjamini-Hochberg correction) for synergistic interactions. We defined suppressor interactions
1404 as those showing a decreased phenotypic score for the recombinant line crossed with the
1405 "second-hit" line compared with recombinant line crossed with the controls.
1406

1407 **S10 Fig. Phenotypic scores of the tested pairwise interactions of *UQCR-C2^{GD11238}* with**
1408 **homologs of "second-hit" or neurodevelopmental genes in *Drosophila* eye.**
1409 *Flynotyper* phenotypic scores of *UQCR-C2^{GD11238}* crossed with RNAi, mutant or overexpression
1410 lines of (**A**) neurodevelopmental genes or genes functionally related with *UQCR-C2* function, (**B**
1411 **and C**) homologs of "second-hits" identified in children with 16p12.1 deletion, and (**D**)
1412 transcriptome targets and functionally related groups identified in RNA-sequencing of *UQCR-C2*
1413 knockdown model. Boxplots represent all data points with median, 25th and 75th percentiles.
1414 Red dotted lines indicate the median of recombinant lines crossed with control. A list of full
1415 genotypes and statistics, including sample size, confidence intervals and p-values, for these
1416 experiments are provided in S1 File and S5 File.
1417

1418 **S11 Fig. Phenotypic scores of the tested pairwise interactions of *Cen^{GD9689}* with homologs of**
1419 **"second-hit" or neurodevelopmental genes in *Drosophila* eye.**
1420 *Flynotyper* phenotypic scores of *Cen^{GD9689}* crossed with RNAi, mutant or overexpression lines of
1421 (**A**) neurodevelopmental genes or genes functionally related with *Cen* function, (**B and C**)
1422 homologs of "second-hits" identified in children with 16p12.1 deletion, and (**D**) transcriptome
1423 targets and functionally related groups identified in RNA-sequencing of *Cen* knockdown model.
1424 Boxplots represent all data points with median, 25th and 75th percentiles. Red dotted lines
1425 indicate the median of recombinant lines crossed with control. A list of full genotypes and

1426 statistics, including sample size, confidence intervals, and p-values, for these experiments are
1427 provided in S1 File and S5 File.

1428

1429 **S12 Fig. Phenotypic scores of the tested pairwise interactions of *Sin*^{GD7027} with homologs of**
1430 **"second-hit" or neurodevelopmental genes in *Drosophila* eye.**
1431 *Flynotyper* phenotypic scores of *Sin*^{GD7027} crossed with RNAi, mutant or overexpression lines of
1432 (**A**) neurodevelopmental genes or genes functionally related with *Sin* function, (**B and C**)
1433 homologs of "second-hits" identified in children with 16p12.1 deletion, and (**D and E**)
1434 transcriptome targets and functionally related groups identified in RNA-sequencing of *Sin*
1435 knockdown model. Boxplots represent all data points with median, 25th and 75th percentiles.
1436 Red dotted lines indicate the median of recombinant lines crossed with control. A list of full
1437 genotypes and statistics, including sample size, confidence intervals and p-values, for these
1438 experiments are provided in S1 File and S5 File.

1439

1440 **S13 Fig. Phenotypic scores of the tested pairwise interactions of *CG14182*^{GD2738} with**
1441 **homologs of "second-hit" or neurodevelopmental genes in *Drosophila* eye.**
1442 *Flynotyper* phenotypic scores of *CG14182*^{GD2738} crossed with RNAi, mutant or overexpression
1443 lines of (**A**) neurodevelopmental genes or genes functionally related with *CG14182* function, (**B**
1444 **and C**) homologs of "second-hits" identified in children with 16p12.1 deletion, and (**D**)
1445 transcriptome targets and functionally related groups identified in RNA-sequencing of *CG14182*
1446 knockdown model. Boxplots represent all data points with median, 25th and 75th percentiles.
1447 Red dotted lines indicate the median of recombinant lines crossed with control. A list of full

1448 genotypes and statistics, including sample size, confidence intervals and p-values, for these
1449 experiments are provided in S1 File and S5 File.

1450

1451 **S14 Fig. Multiple homologs of patient-specific "second-hits" and neurodevelopmental genes**
1452 **modulate phenotypes caused by knockdown of *UQCR-C2*^{GD11238} and *Cen*^{GD9689}.**
1453 Representative brightfield adult eye images and phenotypic scores of eyes from RNAi, mutant or
1454 overexpression lines of neurodevelopmental genes, homologs of genes with "second-hits" in
1455 children with 16p12.1 deletion, and transcriptome targets that significantly enhanced (Enh.) or
1456 suppressed (Supp.) the phenotypes of recombinant lines of *UQCR-C2*^{GD11238} (**A**) or *Cen*^{GD9689} (**B**)
1457 (*p<0.05, two-tailed Mann-Whitney tests with Benjamini-Hochberg correction). Scale bar
1458 represents 100 μm. Boxplots represent all data points with median, 25th and 75th percentiles.
1459 Red dotted lines indicate the median of recombinant lines crossed with control. A list of full
1460 genotypes and statistics, including sample size, confidence intervals and p-values, for these
1461 experiments are provided in S1 File and S5 File.

1462

1463 **S15 Fig. Multiple homologs of patient-specific "second-hits" and neurodevelopmental genes**
1464 **modulate phenotypes caused by knockdown of *CG14182*^{GD2738} and *Sin*^{GD7027}.**
1465 Representative brightfield adult eye images and phenotypic scores of eyes from RNAi, mutant or
1466 overexpression lines of neurodevelopmental genes, homologs of genes with "second-hits" in
1467 children with 16p12.1 deletion, and transcriptome targets that significantly enhanced (Enh.) or
1468 suppressed (Supp.) the phenotypes of recombinant lines of *CG14182*^{GD2738} (**A**) or *Sin*^{GD7027} (**B**)
1469 (*p<0.05, two-tailed Mann-Whitney tests with Benjamini-Hochberg correction). Scale bar

1470 represents 100 μm. Boxplots represent all data points with median, 25th and 75th percentiles.
1471 Red dotted lines indicate the median of recombinant lines crossed with control. A list of full
1472 genotypes and statistics, including sample size, confidence intervals and p-values, for these
1473 experiments are provided in S1 File and S5 File.
1474
1475 **S16 Fig. "Second-hit" genes identified in probands with 16p12.1 deletion.**
1476 Pedigrees of 15 families with the 16p12.1 deletion, highlighting 23 genes with rare secondary
1477 likely-pathogenic mutations (CNVs and SNVs) that were identified in severely affected children
1478 with the 16p12.1 deletion. These 23 genes carrying "second-hit" mutations were selected for
1479 *Drosophila* experiments to test how their decreased expression affects the neurodevelopmental
1480 phenotypes observed for 16p12.1 homologs. Family members who carry either the 16p12.1
1481 deletion or individual genes with "second-hits" are indicated in the pedigrees. Phenotypes
1482 observed for affected children and other family members are indicated below each pedigree.
1483
1484 **S17 Fig. Complex interactions between homologs of "second-hit" genes and 16p12.1**
1485 **homologs.**
1486 (**A-G**) Pedigrees with validated interactions between homologs of genes carrying "second-hits"
1487 in children with the 16p12.1 deletion. Interaction plots and representative brightfield adult eye
1488 images for validated enhancers (Enh.) or suppressors (Supp.) are shown below each pedigree.
1489 Interaction plots show the changes in *Flynotyper* scores (mean ± s.d.) for *GMR-GAL4* control
1490 (grey) or recombinant lines of 16p12.1 homologs crossed with either control line (left) or with
1491 "second-hit" homologs (right). Two-way ANOVA analyses showed epistatic enhancements for
1492 $Cen^{GD9689}/nAChR\alpha6^{GD1045}$ ($p<0.05$ with Benjamini-Hochberg correction). Furthermore, *osa*

1493 suppressed the eye phenotype of each of the four 16p12.1 homologs, and *cac*^{JF02572} suppressed
1494 the eye phenotype of *CG14182*^{GD2738}. Scale bar represents 100 μm. Statistical details of ANOVA
1495 tests are provided in S5 File. A list of full genotypes for fly crosses used in these experiments is
1496 provided in S1 File.
1497
1498 **S18 Fig. *Osa* and *Nipped-A* interact with *CG14182*^{GD2738} through cellular processes during**
1499 **eye development.**
1500 **(A)** Representative brightfield adult eye images show that simultaneous knockdown of
1501 *CG14182*^{GD2738} with *osa*^{JF01207} leads to a suppressed (Supp.) eye phenotype, while simultaneous
1502 knockdown of *Nipped-A*^{HMS00167} leads to synergistic enhancement (Enh.) in eye phenotype
1503 compared to single knockdown of *CG14182*^{GD2738}. Scale bar represents 100 μm. (**B**)
1504 Representative confocal images of third instar larval eye discs stained with DAPI (blue) and anti-
1505 phosphorylated histone-3 (pH3, green) or anti-Dcp-1 (red), markers of cellular proliferation and
1506 apoptosis, respectively. Positive pH3 or Dcp-1 cells were quantified posterior to the
1507 morphogenetic furrow (indicated by white boxes). Simultaneous knockdown of *CG14182*^{GD2738}
1508 with *osa*^{JF01207} led to an increase in the number of pH3 positive cells (n=20, two-tailed Mann-
1509 Whitney, *p= 2.33×10^{-6}) compared to the single knockdown of *CG14182*^{GD2738}. (**C**)
1510 Simultaneous knockdown of *CG14182*^{GD2738} with *Nipped-A*^{HMS00167} led to a significant reduction
1511 in the number of Dcp-1 positive cells compared to single knockdown of *CG14182*^{GD2738} (n=15,
1512 in red, two-tailed, Mann-Whitney, *p=2.54×10^{-5}). Scale bars represent 50 μm. Boxplots
1513 represent all data points with median, 25th and 75th percentiles. Statistical details, including
1514 sample size, confidence intervals and p-values, are provided in S5 File. A list of full genotypes
1515 for fly crosses used in these experiments is provided in S1 File.

1516

1517 **S19 Fig. *setd5* modifies phenotypes observed with knockdown of *polr3e* and *mosmo* in *X.***
1518 ***laevis*.**
1519 **(A)** Representative images stained with anti-tubulin show forebrain (red on control image) and
1520 midbrain (blue) areas of the side injected with morpholino (right, red asterisk), normalized to the
1521 uninjected side (left). Simultaneous knockdown of *polr3e* and *setd5* in *X. laevis* led to decreased
1522 forebrain (n=28, two-tailed student's t-test, *$p=6.01\times10^{-7}$) and midbrain area (*$p=1.67\times10^{-7}$)
1523 compared to knockdown of *polr3e* alone, which were not different to the partial knockdown of
1524 *setd5* alone ($p>0.05$). Scale bar represents 500 µm. (**B**) Normalized axon length of *X. laevis*
1525 tadpoles with simultaneous knockdown of *mosmo* and *setd5* showed decreased axon length
1526 different from the control injected with 22ng of morpholino (n=438, two-tailed, student's t-test,
1527 *$p=2.95\times10^{-7}$) and from individual knockdown of *setd5* (*$p=1.86\times10^{-9}$) or *mosmo* (*$p= 3.34\times10^{-}$
1528 ^{6}), showing a synergistic effect of decreased dosage of the homologs towards neuronal
1529 phenotypes. **(C)** Normalized axon length of *X. laevis* tadpoles with simultaneous knockdown of
1530 *polr3e* and *setd5* showed no change in axon length (two-tailed student's t-test, $p>0.05$). In each
1531 case, the individual knockdown was normalized and compared to the control injected with the
1532 same amount of morpholino. Boxplots represent all data points with median, 25th and 75th
1533 percentiles. Statistical details, including sample size, confidence intervals and p-values, are
1534 provided in S5 File.
1535

1536 **S20 Fig. 16p11.2 genes are more connected to each other than to other genes in the genome.**
1537 Analysis of a human brain-specific network shows higher average pairwise connectivity,
1538 measured as the inverse of the shortest path between two genes, between pairs of 16p11.2 genes

1539 compared to the connectivity of 16p11.2 genes to the rest of the genome (n=25 two-tailed Mann-
1540 Whitney, *p= 6.64×10^{-3}). This trend was not observed for 16p12.1 genes (n=6, p>0.05).
1541 Boxplots represent all data points with median, 25th and 75th percentiles. Statistical details are
1542 provided in S5 File.
1543
1544 **S1 Table. *Drosophila* and *X. laevis* homologs of 16p12.1 genes.**
1545 DIOPT (24) and reciprocal BLAST (70) searches were used to identify fly homologs of 16p12.1
1546 genes. The expression of homologs in the larval central nervous system during development was
1547 assessed using FlyAtlas Anatomy microarray expression data from FlyBase (71).
1548
1549 **S2 Table. "Second-hit" variants identified in families with 16p12.1 deletion and tested for**
1550 **interactions with 16p12.1 homologs.**
1551 Genes carrying "second-hits" were previously identified (9) through exome sequencing and SNP
1552 microarrays in 15 children with the 16p12.1 deletion, and selected as disease-associated genes
1553 carrying rare (ExAC frequency ≤1%) copy-number variants, loss-of-function (frameshift,
1554 stopgain or splicing) mutations, or *de novo* or likely-pathogenic (Phred-like CADD ≥25)
1555 missense mutations.
1556
1557 **S3 Table. Phenotypes observed for individual 16p12.1 homologs in *Drosophila* and *X. laevis***
1558 **models.**
1559 Developmental and neuronal phenotypes observed with individual knockdown of 16p12.1
1560 homologs in *Drosophila* and *X. laevis*.
1561

1562 **S4 Table. Sequences of oligonucleotides used for confirming gene knockdown in *Drosophila***
1563 **and *X. laevis.***
1564
1565 **S5 Table. *X. laevis* morpholino sequences used in this study.**
1566
1567 **S1 File. Stock list and genotypes of *Drosophila* lines used in the study (Excel file).**
1568 This file details genotypes of tissue-specific drivers, and stock centers, stock numbers and
1569 genotypes of RNAi used to knock down the four 16p12.1 homologs, as well as RNAi, mutant, or
1570 overexpression lines for homologs of "second-hit" genes and genes within conserved
1571 neurodevelopmental pathways. Genotypes of recombinant lines of 16p12.1 homologs crossed
1572 with interacting genes are also detailed, as well as the individual controls used for each
1573 experiment. Details of the number of homologs, fly lines, and crosses used for all interaction
1574 experiments are also provided. BDSC: Bloomington Drosophila Stock Center, VDRC: Vienna
1575 Drosophila Stock Center.
1576
1577 **S2 File. Differentially expressed genes and Gene Ontology enrichments for knockdown of**
1578 **16p12.1 homologs (Excel file).**
1579 List of differentially expressed genes, defined as log-fold change >1 or <-1 and false discovery
1580 rate (FDR) <0.05 (Benjamini-Hochberg correction), following RNA sequencing of *Drosophila*
1581 fly heads with *Elav-GAL4*-mediated knockdown of the four 16p12.1 homologs. Human
1582 homologs of differentially-expressed fly genes were identified using DIOPT (24). Enriched Gene
1583 Ontology (GO) and PantherDB terms are also provided for differentially-expressed fly genes and
1584 their human homologs.

1585

1586 **S3 File. Summary of genetic interactions identified with 16p12.1 homologs in *Drosophila***

1587 **(Excel file).**

1588

1589 **S4 File. Connectors of 16p12.1 and 16p11.2 genes identified in a human brain network**

1590 **(Excel file).**

1591

1592 **S5 File. Statistical analysis of experimental data (Excel file).**

1593 This file provides details of all statistical information, including sample size, test statistics, p-

1594 values, and Benjamini-Hochberg FDR corrections for all data shown in the main and

1595 supplemental figures. Details for ANOVA tests include factors, degrees of freedom, tests

1596 statistics, and post-hot pariwise t-tests with Benjamini-Hochberg FDR corrections.

1597

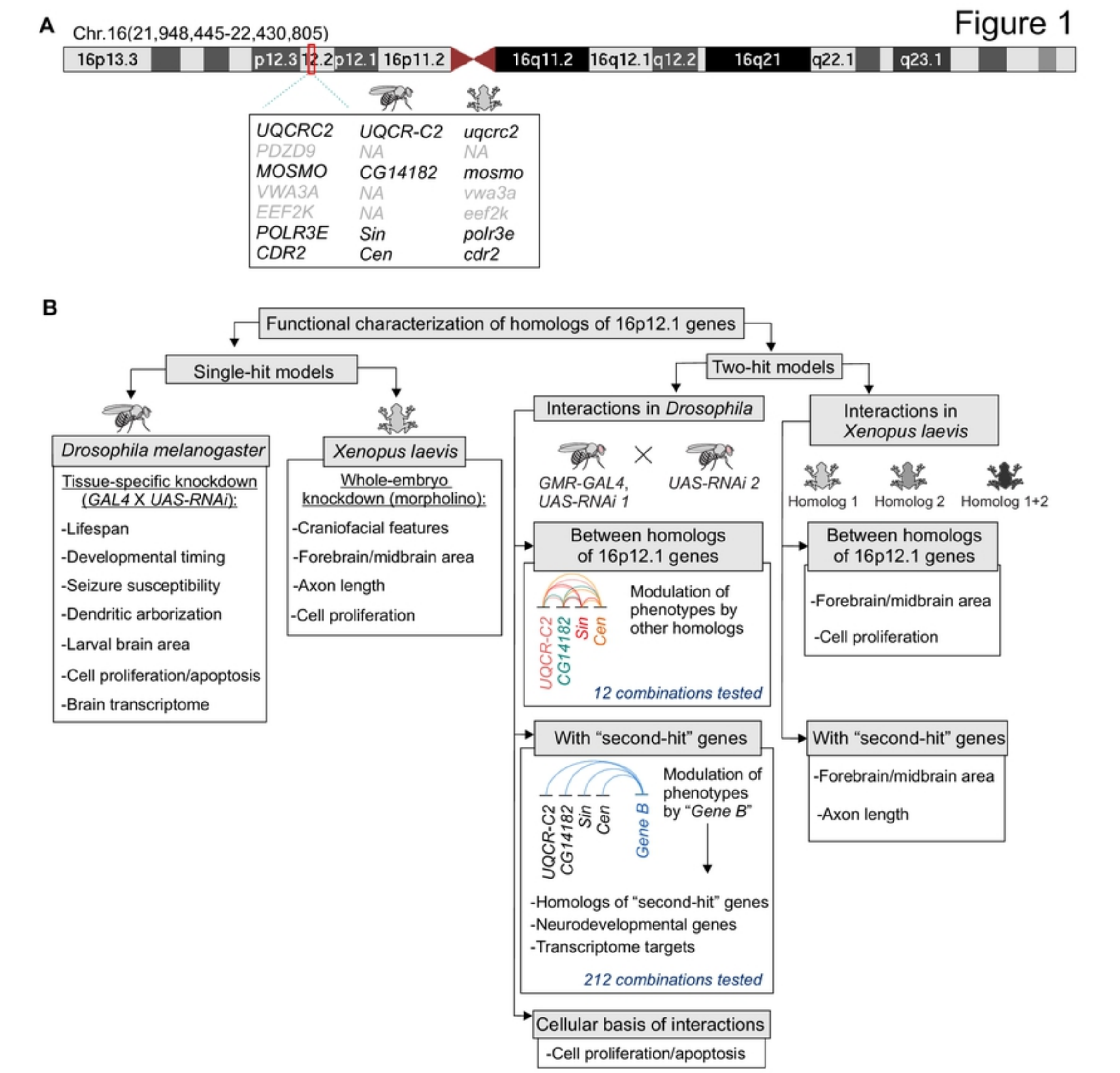
Figure 1
A
Chr.16(21,948,445-22,430,805)
16p13.3
p12.3
12.2
p12.1
16p11.2
16q11.2
16q12.1
q12.2
16q21
q22.1
q23.1
UQCRC2 UQCR-C2 uqcrc2
PDZD9 NA NA
MOSMO CG14182 mosmo
VWA3A NA vwa3a
EEF2K NA eef2k
POLR3E Sin polr3e
CDR2 Cen cdr2
B
Functional characterization of homologs of 16p12.1 genes
Single-hit models
Two-hit models
Drosophila melanogaster
Tissue-specific knockdown (GAL4 X UAS-RNAi):
-Lifespan
-Developmental timing
-Seizure susceptibility
-Dendritic arborization
-Larval brain area
-Cell proliferation/apoptosis
-Brain transcriptome
Xenopus laevis
Whole-embryo knockdown (morpholino):
-Craniofacial features
-Forebrain/midbrain area
-Axon length
-Cell proliferation
Interactions in Drosophila
GMR-GAL4, UAS-RNAi 1
UAS-RNAi 2
Between homologs of 16p12.1 genes
UQCR-C2
CG14182
Sin
Cen
Modulation of phenotypes by other homologs
12 combinations tested
With "second-hit" genes
UQCR-C2
CG14182
Sin
Cen
Gene B
Modulation of phenotypes by "Gene B"
-Homologs of "second-hit" genes
-Neurodevelopmental genes
-Transcriptome targets
212 combinations tested
Cellular basis of interactions
-Cell proliferation/apoptosis
Interactions in Xenopus laevis
Homolog 1
Homolog 2
Homolog 1+2
Between homologs of 16p12.1 genes
-Forebrain/midbrain area
-Cell proliferation
With "second-hit" genes
-Forebrain/midbrain area
-Axon length

Figure1

Figure 2

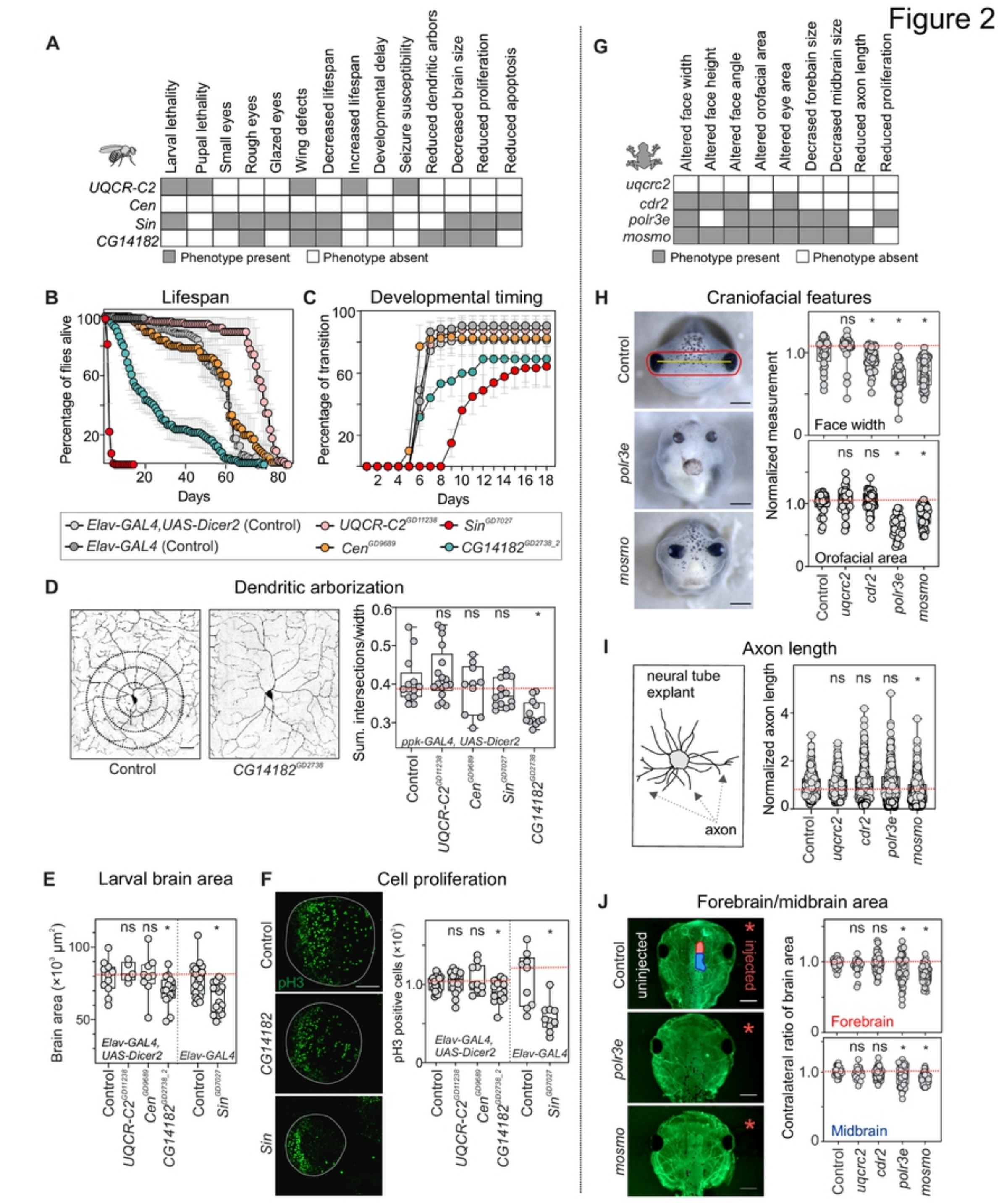

Figure2

Figure 3

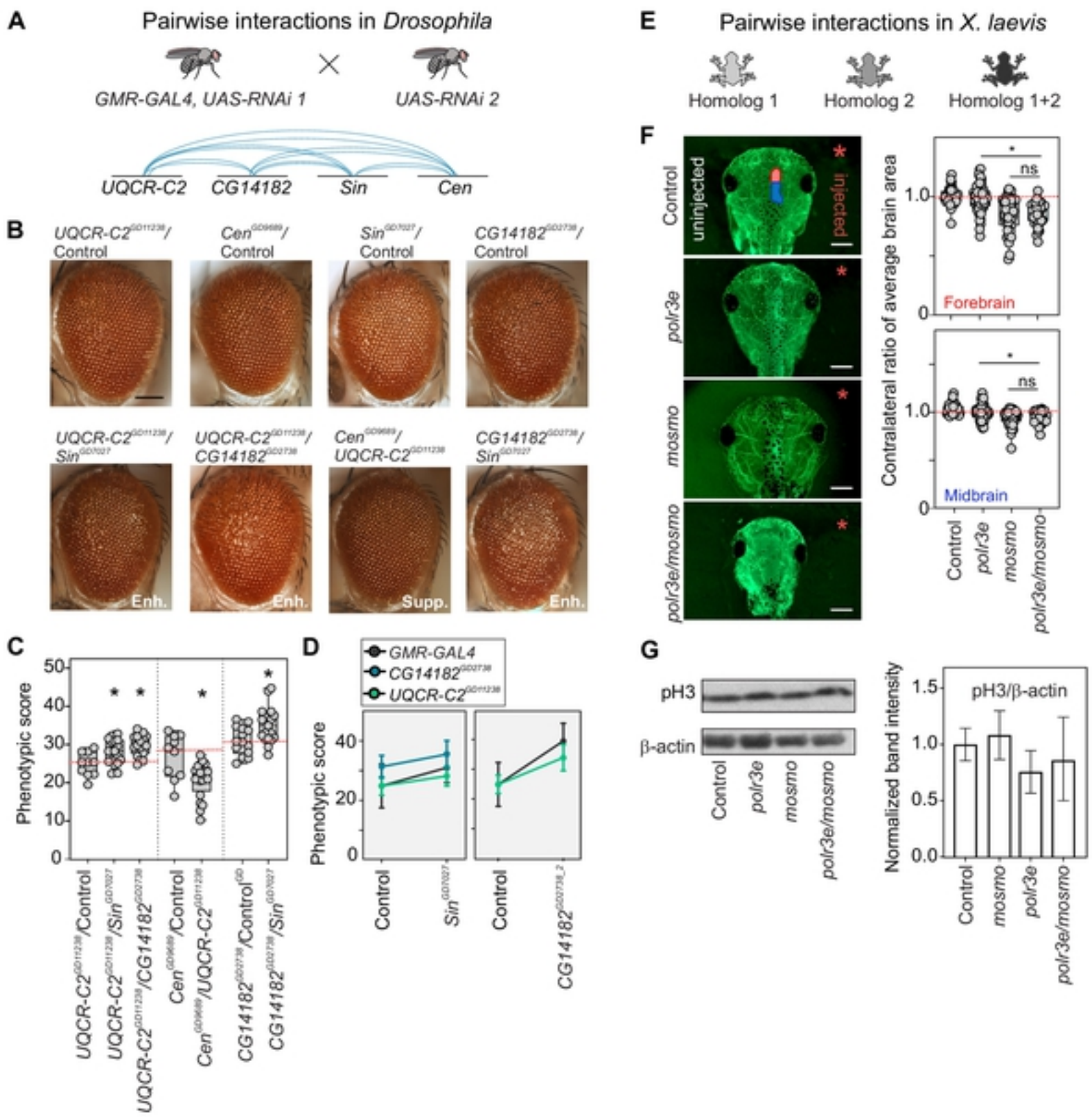

Figure3

Figure 4

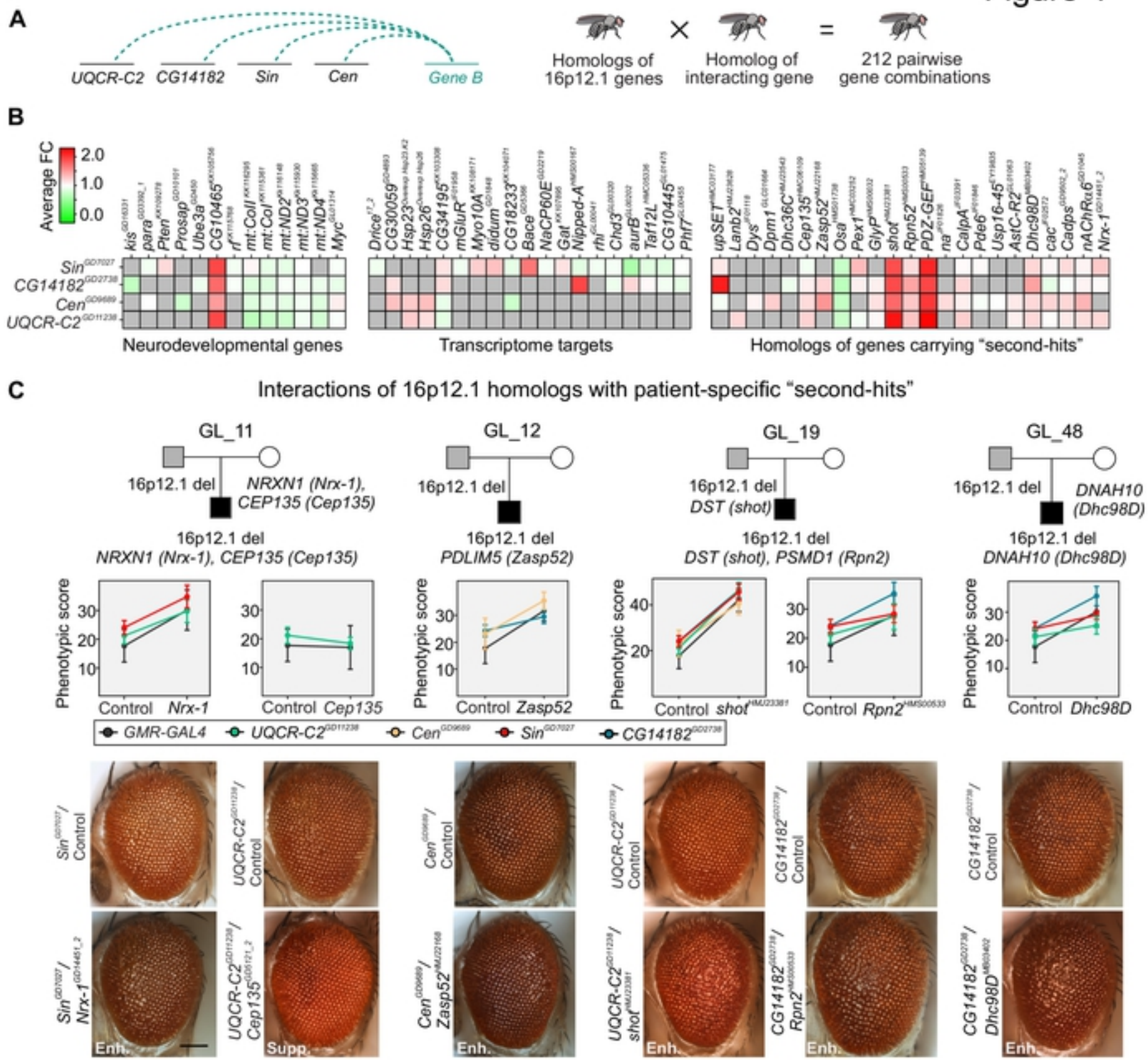

Figure4

Figure 5

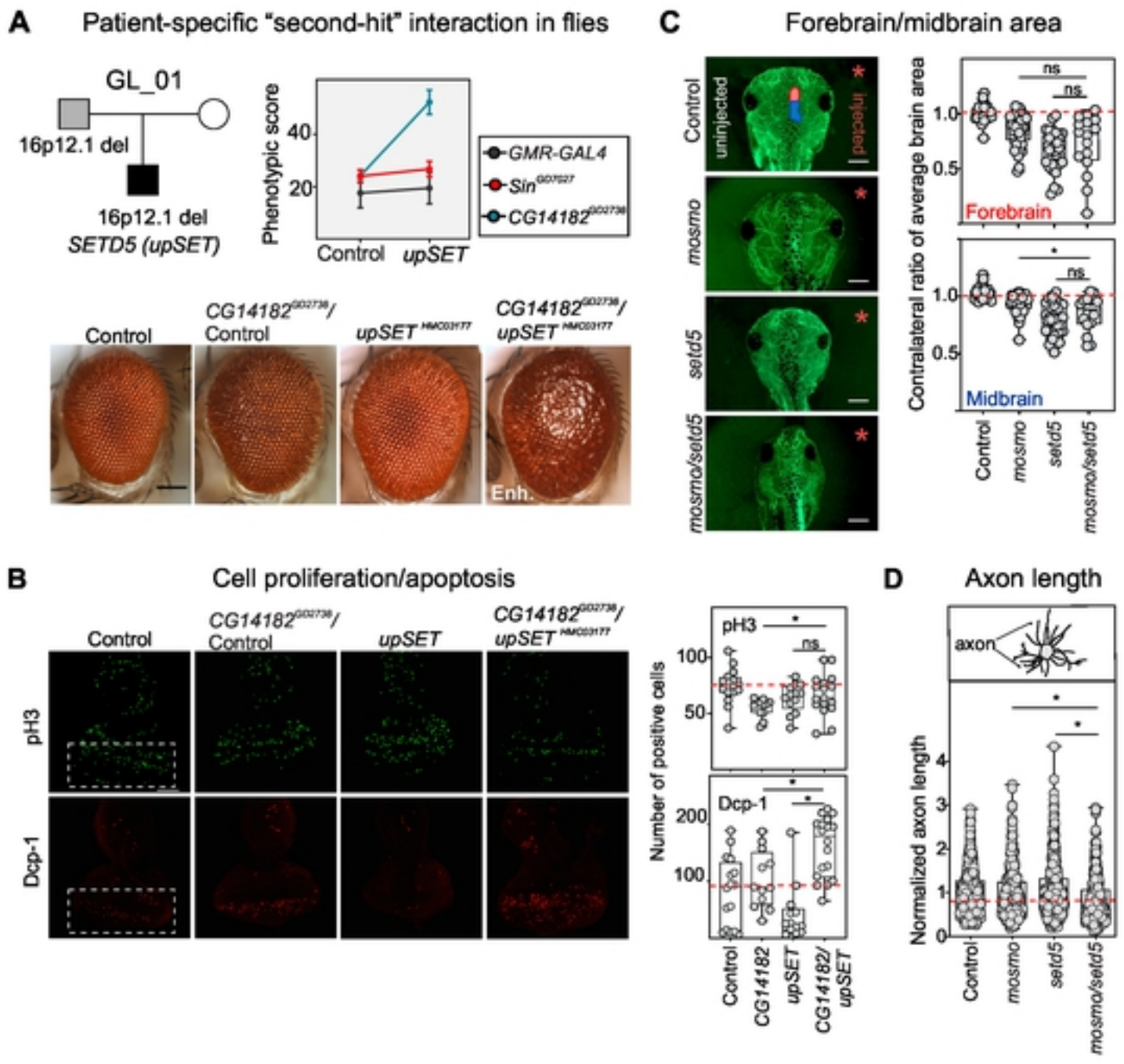

Figure5

Figure 6

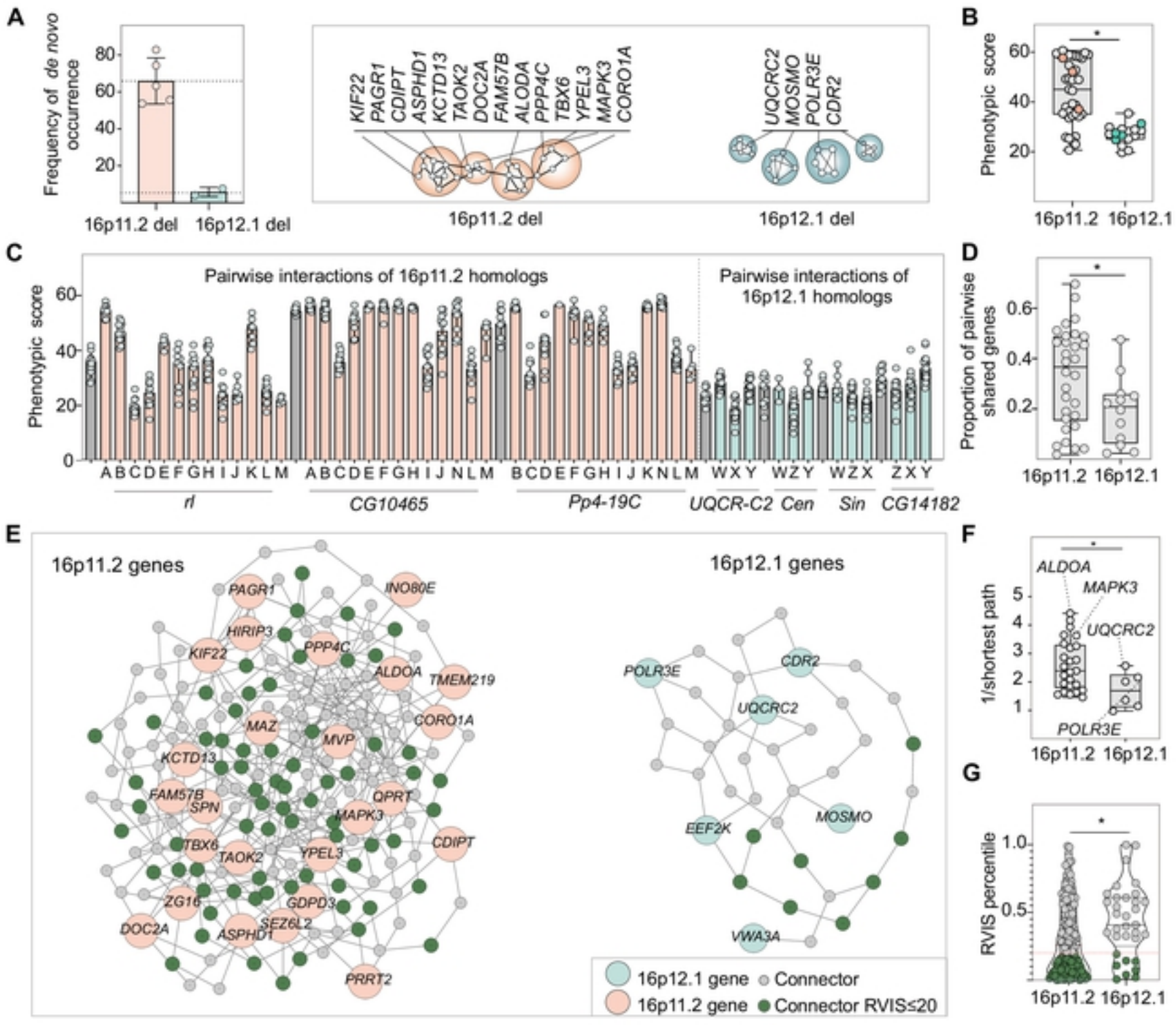

Figure6